

## Unexpected Roles of Triethanolamine in the Photochemical Reduction of CO<sub>2</sub> to Formate by Ruthenium Complexes

Renato N. Sampaio, David C. Grills, Dmitry E. Polyansky, David J. Szalda, and Etsuko Fujita

*J. Am. Chem. Soc.*, **Just Accepted Manuscript** • DOI: 10.1021/jacs.9b11897 • Publication Date (Web): 27 Dec 2019

Downloaded from [pubs.acs.org](https://pubs.acs.org) on December 29, 2019

### Just Accepted

“Just Accepted” manuscripts have been peer-reviewed and accepted for publication. They are posted online prior to technical editing, formatting for publication and author proofing. The American Chemical Society provides “Just Accepted” as a service to the research community to expedite the dissemination of scientific material as soon as possible after acceptance. “Just Accepted” manuscripts appear in full in PDF format accompanied by an HTML abstract. “Just Accepted” manuscripts have been fully peer reviewed, but should not be considered the official version of record. They are citable by the Digital Object Identifier (DOI®). “Just Accepted” is an optional service offered to authors. Therefore, the “Just Accepted” Web site may not include all articles that will be published in the journal. After a manuscript is technically edited and formatted, it will be removed from the “Just Accepted” Web site and published as an ASAP article. Note that technical editing may introduce minor changes to the manuscript text and/or graphics which could affect content, and all legal disclaimers and ethical guidelines that apply to the journal pertain. ACS cannot be held responsible for errors or consequences arising from the use of information contained in these “Just Accepted” manuscripts.

1  
2  
3 Unexpected Roles of Triethanolamine in the Photochemical Reduction of CO<sub>2</sub> to Formate  
4 by Ruthenium Complexes  
5  
6  
7  
8  
9

10 Renato N. Sampaio,<sup>†,\*</sup> David C. Grills,<sup>†</sup> Dmitry E. Polyansky,<sup>†</sup> David J. Szalda,<sup>§</sup> Etsuko Fujita<sup>†,\*</sup>  
11  
12

13  
14 <sup>†</sup>Chemistry Division, Brookhaven National Laboratory, Upton, NY 11973-5000, USA  
15

16 <sup>§</sup>Department of Natural Science, Baruch College, CUNY, New York, NY 10010, USA  
17  
18  
19  
20  
21  
22

23 Abstract  
24

25 A series of 4,4'-dimethyl-2,2'-bipyridyl ruthenium complexes with carbonyl ligands were prepared and  
26 studied using a combination of electrochemical and spectroscopic methods with infrared detection to  
27 provide structural information on reaction intermediates in the photochemical reduction of CO<sub>2</sub> to formate  
28 in acetonitrile (CH<sub>3</sub>CN). An unsaturated 5-coordinate intermediate was characterized, and the hydride  
29 transfer step to CO<sub>2</sub> from a singly-reduced metal hydride complex was observed with kinetic resolution.  
30 While triethanolamine (TEOA) was expected to act as a proton acceptor to ensure the sacrificial behavior  
31 of 1,3-dimethyl-2-phenyl-2,3-dihydro-1*H*-benzo[*d*]imidazole (BIH) as an electron donor, time-resolved  
32 infrared (TRIR) measurements revealed that about 90% of the photogenerated one-electron reduced  
33 complexes undergo unproductive back electron-transfer. Furthermore, TEOA showed the ability to  
34 capture CO<sub>2</sub> from CH<sub>3</sub>CN solutions to form a Zwitterionic alkylcarbonate adduct, and was actively  
35 engaged in key catalytic steps such as the metal hydride formation, the hydride transfer to CO<sub>2</sub> to form  
36 the bound formate intermediate and the dissociation of formate ion product. Collectively, the data provide  
37 an overview on transient intermediates of Ru(II) carbonyl complexes, and emphasize the importance of  
38 considering the participation of TEOA when investigating and proposing catalytic pathways.  
39  
40  
41  
42  
43  
44  
45  
46  
47  
48  
49  
50  
51  
52  
53  
54  
55  
56  
57  
58  
59  
60

## INTRODUCTION

The catalytic reduction of CO<sub>2</sub> to formate is one of the many routes in which CO<sub>2</sub> can be converted into high energy carbon-based products. Molecular catalysts that are capable of carrying out this reaction have promoted a continuous momentum of research activity, which has led to an extensive catalog of metal complexes that have been investigated over the years using electrochemical and/or photochemical approaches.<sup>1-2</sup> While these metal complexes are different in their composition, which controls their physical and chemical properties, they often share a very common condition when employed in photochemical assays for the reduction of CO<sub>2</sub> to formate – *the use of triethanolamine (TEOA)*.<sup>1-3</sup>

Light-driven CO<sub>2</sub> reduction catalysis requires chromophores to harvest light to create excited states that in some cases may be potent enough to transfer high-energy electrons to activate catalysts that are in solution or covalently linked to the chromophore.<sup>1-2, 4</sup> This process occurs in kinetic competition with recombination pathways that often limit the overall efficiency of photoinduced electron transfer and the following catalytic reactions. Hence, to maximize the desired reactions, sacrificial electron donors have been routinely exploited.<sup>1-3</sup> TEOA is oxidized irreversibly around 0.5 V vs NHE and is highly soluble in aqueous and organic solvents, making it a suitable sacrificial reductive quencher for the excited states of chromophores to generate strongly reducing chromophore radicals.<sup>3</sup> In other cases, TEOA is used as a simple Brønsted base to ensure the irreversibility of another, more potent, sacrificial electron donor, by rapidly deprotonating the oxidized donor.<sup>1, 3</sup> Unfortunately, much of the published research ignores the possibility of secondary roles of TEOA in proposed catalytic mechanisms. In a few rare examples, TEOA was found to bind to metal centers of catalysts and to assist in the capture of CO<sub>2</sub> in the ground state;<sup>5-7</sup> however, there have been no substantial indications of whether these findings are more general or if this type of reactivity is a major contribution to the multiple steps of a catalytic cycle.

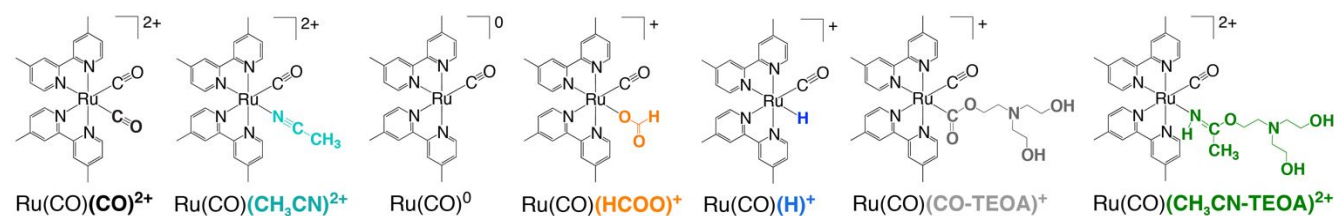


Chart 1. Molecular structures of the Ruthenium(II)-carbonyl complexes of the general, abbreviated formula, Ru(CO)(X)<sup>n+</sup> studied here. All charged complexes were isolated as the PF<sub>6</sub><sup>-</sup> salt.

Herein, we investigate a series of Ru(II) carbonyl complexes, Chart 1, to map out the catalytic pathways and transient intermediates in the photochemical reduction of CO<sub>2</sub> to formate in acetonitrile

(CH<sub>3</sub>CN). This class of catalysts has been studied for over 30 years, with much of the chemistry reported by different groups,<sup>2, 8-15</sup> and yet the investigation of their catalytic intermediates is mostly restricted to steady-state observations with no kinetic information. The carbonyl ligand remains bound and unreactive and serves as an infrared (IR) spectroscopic reporter to identify multiple catalyst forms and their redox states generated by electrochemical and photochemical methods. While the results presented here establish some general conclusions, they also uncover the big picture of photochemical assays that employ TEOA. In CH<sub>3</sub>CN solutions, TEOA fails to efficiently perform its intended task of ensuring the sacrificial behavior of electron donors such as *1,3-dimethyl-2-phenyl-2,3-dihydro-1H-benzo[d]imidazole* (BIH). Time-resolved infrared (TRIR) spectroscopy has revealed that the photochemically generated one-electron reduced species mostly undergo charge recombination within a few microseconds, while only about 10% persist on longer time scales. Unexpected findings also demonstrated that TEOA partakes in critical supporting reactions including the zwitterionic capture of CO<sub>2</sub>, and the assistance in metal hydride formation and formate product dissociation. TEOA also provides an alternative mechanism in which the hydride is transferred to CO<sub>2</sub> to form the bound formato complex, with a 10<sup>6</sup> rate enhancement compared to in the absence of TEOA. The importance of these findings for photochemical CO<sub>2</sub> reduction is discussed.

## EXPERIMENTAL METHODS

*Materials and Synthesis.* Acetonitrile (CH<sub>3</sub>CN, Aldrich, anhydrous, 99.8%), triethanolamine (TEOA, Aldrich, *purris. p.a.*, ≥ 99%), and triethylamine (TEA, Aldrich, ≥ 99%) were dried over activated molecular sieves (Aldrich – 3 Å, beads, 8-12 mesh). Tetrabutylammonium formate salt (TBAHCOO) was prepared according to a reported procedure<sup>16</sup> and dried under reduced pressure. The Ru(II)-carbonyl complexes, [Ru(dmb)<sub>2</sub>(CO)(CO)](PF<sub>6</sub>)<sub>2</sub>, [Ru(dmb)<sub>2</sub>(CO)(CH<sub>3</sub>CN)](PF<sub>6</sub>)<sub>2</sub>, [Ru(dmb)<sub>2</sub>(CO)(HCOO)](PF<sub>6</sub>), and [Ru(dmb)<sub>2</sub>(CO)(H)](PF<sub>6</sub>), where dmb = 4,4'-dimethyl-2,2'-bipyridine,<sup>17-20</sup> and the chromophore [Ru(bpy-OMe)<sub>3</sub>](PF<sub>6</sub>)<sub>2</sub> (where bpy-OMe is 4,4'-dimethoxy-2,2'-bipyridine),<sup>21</sup> were prepared according to published methods. All Ru(II)-carbonyl complexes are abbreviated without (dmb)<sub>2</sub>, i.e., Ru(CO)(CO)<sup>2+</sup>, etc. All chemicals were stored in an inert N<sub>2</sub>-atmosphere glove box before use. <sup>1</sup>H and <sup>13</sup>C NMR spectra were recorded on a Bruker Avance III spectrometer operating at 400.16 and 100.62 MHz, respectively.

*Preparation of [Ru(dmb)<sub>2</sub>(CO)(CH<sub>3</sub>CN-TEOA)](PF<sub>6</sub>)<sub>2</sub>.* 50 mg of [Ru(dmb)<sub>2</sub>(CO)(CH<sub>3</sub>CN)]<sup>2+</sup> was dissolved in 25 mL of acetone containing 2 mL of TEOA. The solution mixture was stirred overnight at

30° C. The initially colorless solution turned dark orange. A precipitate, obtained by adding saturated aqueous  $\text{NH}_4\text{PF}_6$  and cold water, was collected by filtration, and dried under vacuum. Single crystals of  $[\text{Ru}(\text{dmb})_2(\text{CO})(\text{CH}_3\text{CN})](\text{PF}_6)_2$  and  $[\text{Ru}(\text{dmb})_2(\text{CO})\{\text{NHC}(\text{CH}_3)\text{-OC}_2\text{H}_4\}\text{N}\{(\text{C}_2\text{H}_4\text{OH})_2\}](\text{PF}_6)_2$  (i.e.,  $\text{Ru}(\text{CO})(\text{CH}_3\text{CN-TEOA})^{2+}$ ) for X-ray analysis were grown from slow ether diffusion into acetone.

*Preparation of (BIH).* In a round bottom flask, 7 g (36.0 mmol) of 2-phenylbenzimidazole (Aldrich, 97%) was dissolved in 300 mL of acetone containing 3 g (53.5 mmol, 1.5 equiv.) of potassium hydroxide (KOH, Aldrich). To this solution, 6.15 g (43.3 mmol, 1.2 equiv.) of methyl iodide (Aldrich, *ReagentPlus*,  $\geq 99.5\%$ ) was added and the mixture was heated at 50° C for 12 hours. Acetone was removed by rotary evaporation. The resulting oil-like mixture was re-dissolved in 100 mL of ethyl acetate and purified by solvent extraction in 300 mL of Milli-Q water. This process was repeated until the aqueous layer became colorless. After removal of ethyl acetate by rotary evaporation, 2-phenyl-1-methylbenzimidazole was obtained as an oil and confirmed by  $^1\text{H-NMR}$  (400 MHz,  $\text{DMSO-d}_6$ ,  $\delta$ ): 7.86 (d,  $J = 6$  Hz, 2H), 7.69 (d,  $J = 8$  Hz, 1H), 7.64–7.52 (m, 4H), 7.33–7.22 (m, 2H), 3.88 (s, 3H). The second methylation step was performed by dissolving the oil product in 300 mL of ethyl acetate, after which 7.7 g (54.2 mmol, 1.5 equiv. relative to starting material) of methyl iodide was added. This solution was refluxed at 80° C for 12 hours. The precipitate in the reaction mixture was filtered and washed with ethyl acetate multiple times. This solid, 2-phenyl-1,3-dimethylbenzimidazolium iodide, was characterized by  $^1\text{H-NMR}$  (400 MHz,  $\text{DMSO-d}_6$ ,  $\delta$ ): 8.14 (dd,  $J = 6.4, 3.1$  Hz, 2H), 7.9 (d,  $J = 7.6$  Hz, 2H), 7.88–7.73 (m, 5H), 3.89 (s, 6H). The solid was dissolved in 300 mL of methanol, cooled in an ice bath, and then  $\text{NaBH}_4$  (6.8 g, 179.8 mmol, 5 equiv.) was added slowly. After stirring for approximately 30 minutes at room temperature, a white solid was collected by filtration and washed with water. The final product, 1,3-dimethyl-2-phenyl-2,3-dihydro-1*H*-benzo[*d*]imidazole (BIH), was recrystallized from (5:1) ethanol:water and dried under vacuum (5.7 g, 70%), and stored in a  $\text{N}_2$ -atmosphere glove box before use.  $^1\text{H-NMR}$  (400 MHz,  $\text{DMSO-d}_6$ ,  $\delta$ ): 7.55 (dd,  $J = 6.4, 1.9$  Hz, 2H), 7.45 (dd,  $J = 5, 1.9$  Hz, 3H), 6.62 (dd,  $J = 5.4, 3.3$  Hz, 2H), 6.45 (dd,  $J = 5.4, 3.2$  Hz, 2H), 4.87 (s, 1H), 2.48 (s, 6H).

*X-ray diffraction data.* Crystals of  $[\text{Ru}(\text{dmb})_2(\text{CO})(\text{CH}_3\text{CN})](\text{PF}_6)_2$  and  $[\text{Ru}(\text{dmb})_2(\text{CO})\{\text{NHC}(\text{CH}_3)\text{-OC}_2\text{H}_4\}\text{N}\{(\text{C}_2\text{H}_4\text{OH})_2\}](\text{PF}_6)_2$ , were mounted on the end of a glass fiber and the data were collected with a Bruker Kappa Apex II diffractometer. Data collected at 296 K indicated triclinic symmetry and a space group of  $P\bar{1}$  for both crystals. Crystal data and information about the data collection are provided in the Supporting Information.

1  
2  
3 *Electrochemistry.* Cyclic voltammetry measurements were conducted using a BASi Epsilon potentiostat  
4 in a standard three-electrode cell equipped with a glassy carbon (3 mm diameter) working electrode, a  
5 silver (1.6 mm diameter) counter electrode, and a non-aqueous Ag/AgCl pseudo-reference electrode,  
6 equilibrated in a 0.1 M tetrabutylammonium hexafluorophosphate (TBAPF<sub>6</sub>)/CH<sub>3</sub>CN electrolyte solution.  
7 In a typical experiment, 1 mM of the complex of interest was dissolved in electrolyte solution prepared  
8 with dry CH<sub>3</sub>CN (or 1.4 M TEOA/CH<sub>3</sub>CN) and 0.1 M TBAPF<sub>6</sub> salt. All prepared solutions were saturated  
9 with argon prior to the experiment. Cyclic voltammograms of the ferrocenium/ferrocene redox couple,  
10  $E_{1/2}(\text{Fc}^{+/0})$ , were measured before and after each experiment and used to convert the measured reduction  
11 potentials to the normal hydrogen electrode (NHE) scale with the conversion constant,  $E_{1/2}(\text{Fc}^{+/0}) = 0.63$   
12 V vs NHE.<sup>22</sup> Simulations of the cyclic voltammograms were carried out using the DigiSim simulation  
13 software.<sup>23</sup>

14  
15  
16  
17  
18  
19  
20  
21  
22  
23 Infrared spectroelectrochemical (IR-SEC) data were measured in controlled potential electrolysis mode at  
24 fixed applied potentials. A custom-made reflective IR cell equipped with boron-doped diamond working,  
25 platinum counter, and solid-state leakless miniature Ag/AgCl reference (EDAQ) electrodes was coupled  
26 to a Fourier transform infrared (FTIR) spectrometer (Bruker, IFS 66/S) using a VeeMAX III Variable  
27 Angle Specular Reflectance Accessory (Pike Technologies), and the IR absorption changes were  
28 monitored following application of each potential.

29  
30  
31  
32  
33  
34 *Sodium amalgam reductions.* A homemade T-shape glassware equipped with an optical cell was used.  
35 The sodium amalgam (Na–Hg, 0.5% Na in Hg) compartment was separated from the main sample  
36 compartment and optical cell by a frit. Purified anhydrous CH<sub>3</sub>CN was vacuum-transferred to the  
37 glassware, and the apparatus was flame-sealed. Stepwise reductions were obtained by gradually  
38 transferring the solution into the amalgam compartment through the frit and returning it to the main  
39 compartment while monitoring the changes in ultraviolet-visible absorption.

40  
41  
42  
43  
44 *Infrared spectroscopy.* Steady-state mid-infrared absorption spectra were measured on a Thermo Nicolet  
45 Nexus 670 FTIR spectrometer with a spectral resolution of 2 cm<sup>-1</sup>.

46  
47  
48  
49 *Time-resolved infrared (TRIR) spectroscopy.* TRIR measurements were performed in the 1978 – 1870  
50 cm<sup>-1</sup> region using a CW external-cavity quantum cascade laser (EC-QCL, Daylight Solutions, 21052-  
51 MHF-012) as the mid-infrared probe light source; or in the 2120 – 2005 cm<sup>-1</sup> region using EC-QCL model  
52 21049-MHF. A Nd:YAG pulsed laser (SpectraPhysics, Quanta-Ray LAB-170-10, 8-10 ns FWHM) was  
53 used as the excitation light source tuned to 532 nm using a built-in second harmonic generator. The mid-  
54  
55  
56  
57

1  
2  
3 IR beam was split into reference and probe beams, with the latter passing through the IR cell. These beams  
4 were directed onto a matched pair of fast rise time IR detectors (Kolmar Technologies, Inc., KMPV9-0.5-  
5 J2, DC-20 MHz). The analog signals were simultaneously digitized on an oscilloscope (Teledyne LeCroy  
6 HDO 4034, 12-bit, 350 MHz, 2.5 GS/s) and normalized to remove noise from laser intensity fluctuations.  
7  
8 For a more complete description of the TRIR instrumentation, the authors suggest previously reported  
9 work in which it was applied to pulse radiolysis measurements.<sup>24</sup> Solutions for the TRIR experiments  
10 were prepared in an inert N<sub>2</sub>-atmosphere glove box using an airtight demountable liquid IR cell equipped  
11 with CaF<sub>2</sub> windows (Harrick Scientific, DLC-S25, pathlength  $d = 1.9$  mm). TRIR experiments did not  
12 cover the 2005 – 1978 cm<sup>-1</sup> infrared region due to a gap between the tuning ranges of the two EC-QCLs.  
13  
14

15  
16  
17  
18  
19 *Computational methods.* Density functional theory calculations were performed using the Gaussian 09  
20 software package.<sup>25</sup> Ground-state geometries of the singly- and doubly-reduced complexes were  
21 optimized using the M06 hybrid meta exchange-correlation functional,<sup>26</sup> with the Integral Equation  
22 Formalism Polarizable Continuum Model (IEF-PCM)<sup>27</sup> for CH<sub>3</sub>CN as solvent. The LANL08 relativistic  
23 effective core potential (RECP) and associated uncontracted basis set was used to describe the Ru-  
24 atoms,<sup>28-29</sup> and 6-31G(d) was used for all other atoms. Transition state calculations were performed under  
25 these same conditions. Single point energy calculations at the 6-311++G(2df,p) level were performed for  
26 all optimized structures and transition states to evaluate the electronic energies. Frequency calculations of  
27 the optimized structures were conducted to ensure that all local minima exhibited real frequencies,  
28 whereas transition states displayed only one imaginary frequency. Frequency calculations were also used  
29 to evaluate the Gibbs free energies of the local minima and transition states. For all calculations, the Ru(II)  
30 carbonyl complexes had bpy ligands instead of dmb in order to avoid undesired negative frequencies  
31 occurring at the methyl groups. Cartesian coordinates for optimized transition states are included in the  
32 Supporting Information.  
33  
34  
35  
36  
37  
38  
39  
40  
41  
42

## 43 44 RESULTS

45  
46 Early work has demonstrated that TEOA reacts with one of the carbonyl ligands of Ru(CO)(CO)<sup>2+</sup> via  
47 a nucleophilic attack on the carbonyl-carbon by a deprotonated TEOA-hydroxy group to yield a complex  
48 with a CO-TEOA adduct coordinated to the metal, Ru(CO)(CO-TEOA)<sup>+</sup> (Figure S1).<sup>14</sup> This process is  
49 analogous to the Lewis acid-base equilibrium between metal carbonyls and metalcarboxylic acids, M-  
50 CO<sup>n</sup> + OH<sup>-</sup> ⇌ M-COOH<sup>n-1</sup>. The equilibrium between Ru(CO)(CO)<sup>2+</sup> and OH<sup>-</sup> or TEOA was investigated  
51 through titration measurements of the base while monitoring the changes in the ultraviolet-visible (UV-  
52  
53  
54  
55  
56  
57  
58  
59  
60

vis) absorbance spectrum. Equilibrium constants of  $3 \times 10^4 \text{ M}^{-1}$  and  $2 \times 10^2 \text{ M}^{-1}$  were obtained for  $\text{OH}^-$  and TEOA, respectively (see Figure S1 for the TEOA data). For reasons that are relevant to the discussion in this work and to other related published results,<sup>14, 30</sup> any reference to the  $\text{Ru}(\text{CO})(\text{CO-TEOA})^+$  complex and its characterization, will hereafter imply the addition of the parent  $\text{Ru}(\text{CO})(\text{CO})^{2+}$  catalyst to a concentrated (1.4 M) TEOA/ $\text{CH}_3\text{CN}$  solution (1:4 v:v). Addition of TEOA to solutions containing other forms of the catalyst did not cause noticeable reactivity, with the exception of the solvento complex,  $\text{Ru}(\text{CO})(\text{CH}_3\text{CN})^{2+}$ , for which the coordinated solvent of  $\text{Ru}(\text{CO})(\text{CH}_3\text{CN})^{2+}$  slowly underwent partial solvolysis of the nitrile to form the bound imino ester adduct,  $\text{Ru}(\text{CO})(\text{CH}_3\text{CN-TEOA})^{2+}$  (Figure S2), in a manner similar to that previously observed for a related rhenium complex.<sup>5</sup> This complex was later prepared and isolated as a single crystal, allowing X-ray crystallographic confirmation of the proposed molecular structure. Note that in this case, while the TEOA is deprotonated similar to in  $\text{Ru}(\text{CO})(\text{CO-TEOA})^+$ , the proton remains in the complex, bound to the N-atom of  $\text{CH}_3\text{CN}$ . Crystallographic data are discussed in the Supporting Information.

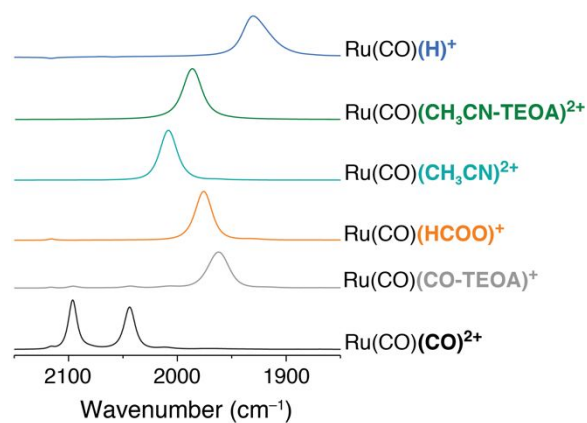


Figure 1. Steady-state infrared absorption spectra of the Ru(II)-carbonyl complexes in the  $\nu(\text{CO})$  carbonyl stretching region in  $\text{CH}_3\text{CN}$ .

Infrared spectra were measured for all  $\text{Ru}(\text{CO})(\text{X})^{n+}$  complexes at frequencies that report on the carbonyl stretching vibrations,  $\nu(\text{CO})$  (Figure 1 and Table 1).  $\text{Ru}(\text{CO})(\text{CO})^{2+}$  shows two vibrational bands centered around  $2100 - 2000 \text{ cm}^{-1}$  associated with symmetric and asymmetric stretching modes of the cis terminal carbonyl groups. Substitution of one carbonyl with other groups that have been identified as intermediates in the catalytic  $\text{CO}_2$  reduction cycle led to red shifts of the remaining CO stretching frequency due to an inductive effect on the  $\pi$ -electron back donation from the metal to the carbonyl group. Molar absorption coefficients ( $\epsilon$ ) at the  $\nu(\text{CO})$  maxima were measured as  $1650 \pm 50 \text{ M}^{-1} \text{ cm}^{-1}$  for

Ru(CO)(HCOO)<sup>+</sup>, Ru(CO)(CO-TEOA)<sup>+</sup> and Ru(CO)(H)<sup>+</sup>, while the higher energy  $\nu(\text{CO})$  of Ru(CO)(CO)<sup>2+</sup> and the  $\nu(\text{CO})$  of Ru(CO)(CH<sub>3</sub>CN)<sup>2+</sup> displayed slightly larger values ( $1800 \pm 50 \text{ M}^{-1} \text{ cm}^{-1}$ ).

Table 1. Experimentally determined carbonyl vibrations,  $\nu(\text{CO})$ , of the studied Ru(CO)(X)<sup>n+</sup> complexes in their resting state (RS) and respective singly- and doubly-reduced states, in CH<sub>3</sub>CN solution.

Complex	$\nu(\text{CO})$ (cm <sup>-1</sup> )		
	RS	1 <sup>st</sup> red	2 <sup>nd</sup> red
Ru(CO)(CH <sub>3</sub> CN) <sup>2+</sup>	2008	1970 <sup>a</sup>	
Ru(CO)(CO) <sup>2+</sup>	2096/2040	2067/2008 <sup>b</sup>	
Ru(CO)(H) <sup>+</sup>	1930	1894 <sup>a</sup>	1862 <sup>a</sup>
Ru(CO)(HCOO) <sup>+</sup>	1976	1938 <sup>a</sup>	
Ru(CO)(CO-TEOA) <sup>+</sup>	1962	1928 <sup>b</sup>	

<sup>a</sup>Determined from spectroelectrochemical methods. <sup>b</sup>Obtained from TRIR experiments.

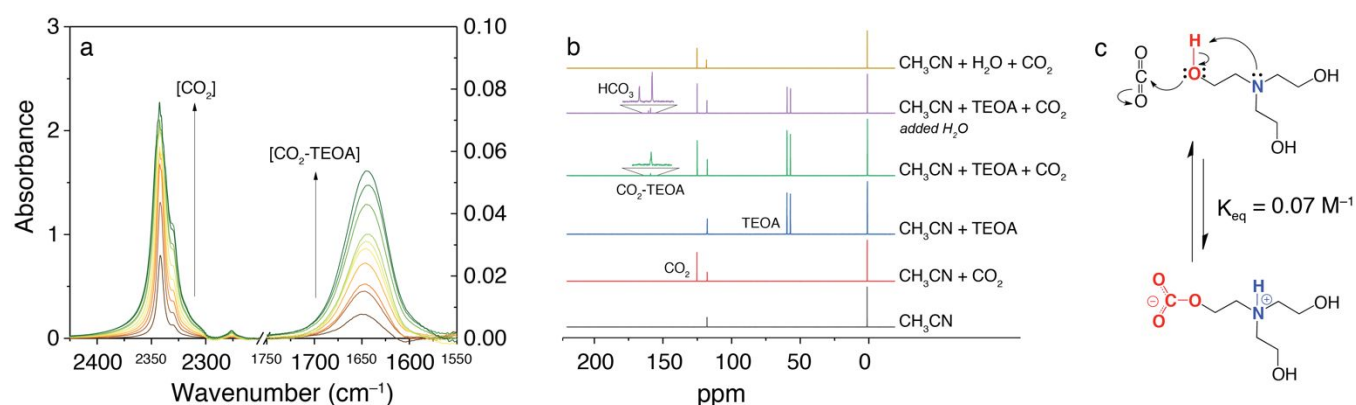


Figure 2. (a) Infrared spectra of a 0.75 M TEOA/CH<sub>3</sub>CN solution mixture measured while titrating in known amounts of CO<sub>2</sub>. (b) <sup>13</sup>C-NMR spectra of the indicated solutions. (c) Reaction scheme for the formation of the CO<sub>2</sub>-TEOA zwitterion.

The direct reaction of TEOA with CO<sub>2</sub> in CH<sub>3</sub>CN was observed by the appearance of a carbonyl vibration at  $1648 \text{ cm}^{-1}$ , which followed a linear dependence on the concentration of dissolved CO<sub>2</sub> monitored at  $2342 \text{ cm}^{-1}$  (Figure 2a). This new IR band appears in a region known for the asymmetric C=O stretching vibrations of bicarbonate in CH<sub>3</sub>CN, at  $1685$  and  $1646 \text{ cm}^{-1}$ ,<sup>16, 31</sup> and the <sup>13</sup>C-NMR spectrum (Figure 2b) with added <sup>13</sup>CO<sub>2</sub> shows a resonance at  $158.9 \text{ ppm}$  typical of organic carbonates.<sup>32</sup> The presence of equilibrated carbonates formed due to residual water was ruled out by further addition of water which resulted in the formation of a new resonance at  $160.5 \text{ ppm}$  consistent with inorganic carbonate.<sup>33</sup> Based on these results, a preliminary assumption that CO<sub>2</sub> may be reacting with TEOA to form a zwitterionic alkylcarbonate structure, CO<sub>2</sub>-TEOA, shown in Figure 2c seems reasonable. Similar

chemistry has precedent in CO<sub>2</sub>-binding organic liquids that contain an alcohol and an amidine or guanidine base and chemically bind CO<sub>2</sub> to form stable zwitterionic adducts.<sup>31, 34</sup> The infrared spectra and <sup>13</sup>C-NMR characterization of these reported adducts support the assignment established here for CO<sub>2</sub>-TEOA.<sup>32</sup> While tertiary amines have a relatively strong Brønsted basicity to act as proton acceptors,<sup>35</sup> the N-atom of TEOA alone is not basic enough to deprotonate its terminal OH groups. This process becomes more thermodynamically favorable by considering a concerted *proton-coupled nucleophilic attack* of CO<sub>2</sub> (Figure 2c). Quantitative analysis of the data in Figure 2a provided an equilibrium constant,  $K_{\text{eq}} = 0.07 \text{ M}^{-1}$ , for the zwitterionic capture of CO<sub>2</sub> by TEOA in CH<sub>3</sub>CN (see SI for details).

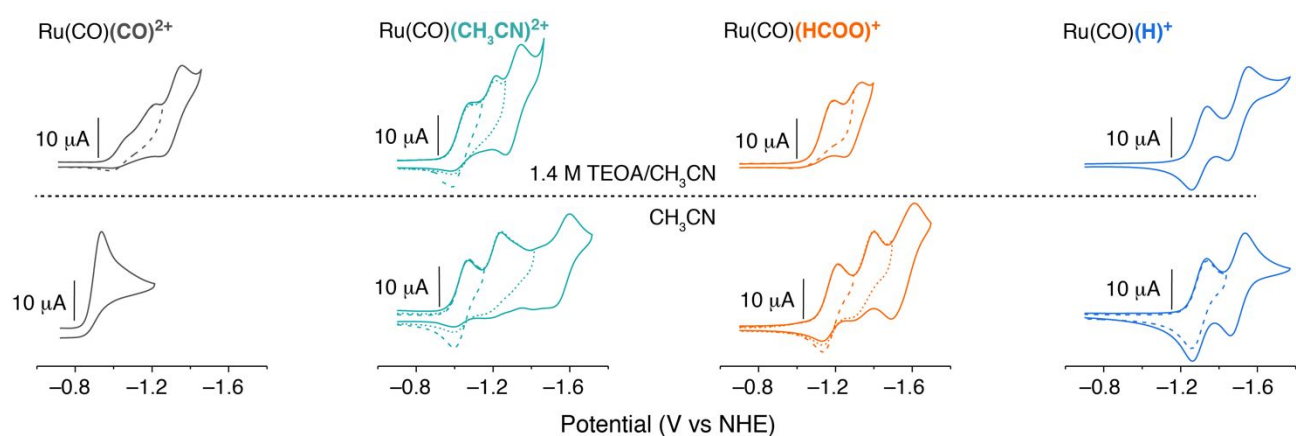


Figure 3. Cyclic voltammograms for 1 mM solutions of the indicated Ru(CO)(X)<sup>n+</sup> complexes measured at 100 mV/s scan rate, in 0.1 M TBAPF<sub>6</sub> CH<sub>3</sub>CN (bottom) or 1.4 M TEOA/CH<sub>3</sub>CN (top) electrolyte solution.

**(Spectro)Electrochemistry.** Cyclic voltammograms for 1 mM solutions of the indicated Ru(CO)(X)<sup>n+</sup> complexes are shown in Figure 3 in argon-saturated CH<sub>3</sub>CN with (top) or without (bottom) added 1.4 M TEOA. At a scan rate of 100 mV s<sup>-1</sup>, Ru(CO)(CO)<sub>2</sub><sup>2+</sup> undergoes an irreversible two-electron reduction at  $E_{1/2} = -0.91 \text{ V vs NHE}$ .<sup>9</sup> The solvento complex, Ru(CO)(CH<sub>3</sub>CN)<sub>2</sub><sup>2+</sup>, shows two reductions at  $E_{1/2} = -1.03$  and  $-1.23 \text{ V vs NHE}$ , both of which were quasi-reversible and scan rate dependent (Figure S5). Similar scan rate dependence on the reversibility of the one- and two-electron reductions was observed for the formate complex, Ru(CO)(HCOO)<sup>+</sup>, at  $E_{1/2} = -1.16$  and  $-1.36 \text{ V vs NHE}$  (Figure S6). Reversible redox chemistry was observed for the Ru(CO)(H)<sup>+</sup> complex in a 25-5000 mV s<sup>-1</sup> scan rate range, with two sequential one-electron reductions appearing at  $E_{1/2} = -1.30$  and  $-1.50 \text{ V vs NHE}$ . In all cases, the redox chemistry was characteristic of ligand-based reductions, and the couples with irreversible behavior for Ru(CO)(CH<sub>3</sub>CN)<sub>2</sub><sup>2+</sup> and Ru(CO)(HCOO)<sup>+</sup> reported on ligand (CH<sub>3</sub>CN, or HCOO<sup>-</sup>) labilization.<sup>9, 11</sup> The

Ru(CO)(CH<sub>3</sub>CN)<sup>2+</sup> and Ru(CO)(HCOO)<sup>+</sup> showed a third couple that is reversible with  $E_{1/2} = -1.55$  V vs NHE. All formal reduction potentials are compiled in Table 2. The redox properties of Ru(CO)(X)<sup>n+</sup> changed substantially in the presence of TEOA (Figure 3, top). With the exception of Ru(CO)(H)<sup>+</sup>, each complex showed an irreversible reduction followed by a reversible couple at  $E_{1/2} = -1.30$  V vs NHE. This second reduction is identical in potential to the first reduction of the hydrido complex, Ru(CO)(H)<sup>+</sup> (see below).

Table 2. Reduction potentials of the Ru(CO)(X)<sup>n+</sup> complexes in CH<sub>3</sub>CN.

Complex	$E_{1/2}$ (V vs NHE) <sup>a</sup>		
	2+/+	+/0	0/-
Ru(CO)(CH <sub>3</sub> CN) <sup>2+</sup>	-1.03 <sup>b</sup>	-1.23 <sup>b</sup>	
Ru(CO)(CO) <sup>2+</sup>	-0.91 <sup>c</sup>	< -0.91	
Ru(CO)(H) <sup>+</sup>		-1.30	-1.50
Ru(CO)(HCOO) <sup>+</sup>		-1.1 <sup>b</sup>	-1.36 <sup>b</sup>
Ru(CO) <sup>0</sup>			-1.55

<sup>a</sup>Potentials were converted to NHE using the conversion constant,  $E_{1/2}(\text{Fc}^{+/0}) = 0.63$  V vs NHE. <sup>b</sup>Quasi-reversible reduction, <sup>c</sup>Irreversible reduction, reported value corresponds to the cathodic peak potential at 100 mV s<sup>-1</sup> scan rate.

Simulation of the scan-rate-dependent data for the Ru(CO)(HCOO)<sup>+</sup> complex allowed kinetic modeling of the formate dissociation triggered by the 1<sup>st</sup> and 2<sup>nd</sup> reductions (Figure S6 and Table S5). The mechanism was modeled with a combination of sequential electrochemical reduction and chemical steps that accounts for the dissociation of HCOO<sup>-</sup> (see Figure S6 and Table S4 for details). The loss of formate from the singly-reduced Ru(CO)(HCOO)<sup>+</sup> in CH<sub>3</sub>CN is sluggish with a forward rate constant,  $k_f = 0.07$  s<sup>-1</sup> and is thermodynamically unfavorable, with  $K_{\text{eq}} = 0.03$  M. Attempts to resolve the kinetics for formate loss in 1.4 M TEOA/CH<sub>3</sub>CN were unsuccessful because the data were nearly scan rate independent, suggesting the dissociation was too fast to measure electrochemically. However, lowering the TEOA concentration to 50 mM was found to be sufficient to decelerate the dissociation of formate, allowing simulation of  $k_f$  1 s<sup>-1</sup> for the singly-reduced species. Under this condition, the formate dissociation at the first electron reduction is thermodynamically allowed with  $K_{\text{eq}} = 3.9$ , and is accelerated by up to 2 orders of magnitude for the same reaction when compared to in the absence of TEOA.

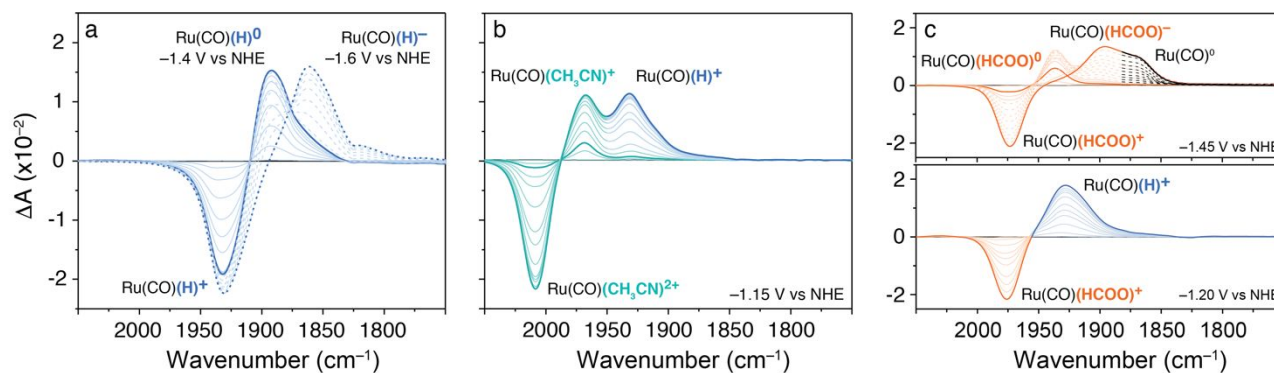


Figure 4. Absorption changes during reductive spectroelectrochemical measurements in  $\text{CH}_3\text{CN}$  on (a)  $\text{Ru}(\text{CO})(\text{H})^+$ , (b)  $\text{Ru}(\text{CO})(\text{CH}_3\text{CN})^{2+}$ , and (c)  $\text{Ru}(\text{CO})(\text{HCOO})^+$  in the presence of 0.5 M TBAHCOO (top) or 1.4 M TEOA (bottom), all containing 0.1 M  $\text{TBAPF}_6$  as the supporting electrolyte.

Spectroelectrochemical data for the  $\text{Ru}(\text{CO})(\text{X})^{n+}$  complexes are shown in Figure 4. Upon reduction of  $\text{Ru}(\text{CO})(\text{H})^+$  at  $-1.4$  V vs NHE, the  $\nu(\text{CO})$  at  $1930$   $\text{cm}^{-1}$  was lost concomitantly with the growth of a new  $\nu(\text{CO})$  vibration at  $1894$   $\text{cm}^{-1}$  assigned to  $\text{Ru}(\text{CO})(\text{H})^0$ . The doubly-reduced  $\text{Ru}(\text{CO})(\text{H})^-$  was generated thereafter by application of  $-1.6$  V vs NHE, with a new  $\nu(\text{CO})$  at  $1862$   $\text{cm}^{-1}$ . The intermediate  $\text{Ru}(\text{CO})(\text{H})^0$  and initial  $\text{Ru}(\text{CO})(\text{H})^+$  complexes were fully recovered upon stepwise re-oxidation, while maintaining isosbestic points consistent with those observed in the reductive steps. Reduction of the  $\text{Ru}(\text{CO})(\text{CH}_3\text{CN})^{2+}$  complex at  $-1.15$  V vs NHE initially generated  $\text{Ru}(\text{CO})(\text{CH}_3\text{CN})^+$  with  $\nu(\text{CO})$  at  $1970$   $\text{cm}^{-1}$ , followed by the subsequent appearance of another band at lower wavenumber. This resultant  $\nu(\text{CO})$  vibration was characteristic of the  $\text{Ru}(\text{CO})(\text{H})^+$  resting state at  $1930$   $\text{cm}^{-1}$ . Spectroelectrochemical data for  $\text{Ru}(\text{CO})(\text{HCOO})^+$  were collected with 0.5 M TBAHCOO to minimize the effect of  $\text{HCOO}^-$  dissociation (Figure 4c, top). At an applied potential of  $-1.45$  V vs NHE, the initial absorption changes were consistent with formation of the singly-reduced  $\text{Ru}(\text{CO})(\text{HCOO})^0$  with  $\nu(\text{CO})$  at  $1938$   $\text{cm}^{-1}$ . At longer equilibration times, the singly-reduced  $\text{Ru}(\text{CO})(\text{HCOO})^0$  was converted to a set of two overlapping vibrations that appeared in the  $1925$ – $1850$   $\text{cm}^{-1}$  region. Spectral fitting with a sum of three Voigt functions afforded peaks at  $1900$   $\text{cm}^{-1}$  and  $1870$   $\text{cm}^{-1}$ , which could not be assigned to any of the known  $\nu(\text{CO})$  previously characterized for the  $\text{Ru}(\text{CO})(\text{X})^{n+}$  complexes. The final amplitudes of the new peaks at  $1900$   $\text{cm}^{-1}$  and  $1870$   $\text{cm}^{-1}$  were potential-dependent and reported on the equilibrated amounts that were generated after reduction, but their relative amplitudes remained constant regardless of the potential applied. This latter behavior was indicative of an equilibrium being established between these two species. While spectroelectrochemical reduction of  $\text{Ru}(\text{CO})(\text{HCOO})^+$  in TBAHCOO-containing electrolyte did not

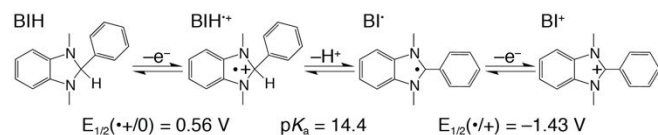
1  
2  
3 produce the  $\text{Ru}(\text{CO})(\text{H})^+$ , experiments performed in 0.1  $\text{TBAPF}_6/\text{CH}_3\text{CN}$  with or without TEOA resulted  
4 in the immediate formation of  $\text{Ru}(\text{CO})(\text{H})^+$  (Figure 4c, bottom).  
5  
6

7 Sodium-amalgam (Na-Hg) reductions of the  $\text{Ru}(\text{CO})(\text{H})^+$  and  $\text{Ru}(\text{CO})(\text{CH}_3\text{CN})^{2+}$  provided UV-vis  
8 characterization of the 5-coordinated  $\text{Ru}(\text{CO})^0$  complex (Figure S7). The redox states of each complex  
9 were monitored by the changes in isosbestic points during the stepwise reduction. The singly- and doubly-  
10 reduced forms of the  $\text{Ru}(\text{CO})(\text{H})^+$  showed clear ligand radical character with a strong band in the 450 –  
11 600 nm region. While the IR-SEC data suggest that the doubly-reduced  $\text{Ru}(\text{CO})(\text{CH}_3\text{CN})^0$  dissociates  
12  $\text{CH}_3\text{CN}$  to form the 5-coordinate  $\text{Ru}(\text{CO})^0$  which may react with a proton to form  $\text{Ru}(\text{CO})(\text{H})^+$ , the UV-  
13 vis spectrum obtained at the 2<sup>nd</sup> electron reduction of  $\text{Ru}(\text{CO})(\text{CH}_3\text{CN})^{2+}$  by Na-Hg exhibited clear ligand  
14 radical character with no indication of reactivity with protons, i.e.  $\text{Ru}(\text{CO})^0 + \text{H}^+ \rightarrow \text{Ru}(\text{CO})(\text{H})^+$ .  
15 Therefore, a direct comparison of these two spectra suggests that the 5-coordinate  $\text{Ru}(\text{CO})^0$  complex was  
16 isolated in the Na-Hg experiment due to the strictly anhydrous conditions and absence of electrolyte  
17 ( $\text{TBAPF}_6$ ) salts. The third reduction of  $\text{Ru}(\text{CO})(\text{CH}_3\text{CN})^{2+}$  showed increased ligand radical character with  
18 absorption changes that were notably different from those measured for  $\text{Ru}(\text{CO})(\text{H})^0$ . This reduction was  
19 instead assigned to the formation of  $\text{Ru}(\text{CO})^-$ , which is consistent with the reversible reduction at  $E_{1/2} = -$   
20 1.55 V vs NHE that was common among  $\text{Ru}(\text{CO})(\text{CH}_3\text{CN})^{2+}$  and  $\text{Ru}(\text{CO})(\text{HCOO})^+$  initial species and  
21 therefore characterizes the reversible redox couple,  $\text{Ru}(\text{CO})^{0/-}$ .  
22  
23  
24  
25  
26  
27  
28  
29  
30  
31  
32

33 **Time-Resolved IR.** Isolation of various catalyst forms that are proposed as reaction intermediates in the  
34 reduction of  $\text{CO}_2$  allowed for their spectroscopic and electrochemical characterization. Each of these may  
35 have an active role in the catalytic pathways through their initial resting state or reduced states. By using  
36 transient absorption measurements, the singly-reduced states of  $\text{Ru}(\text{CO})(\text{X})^{n+}$  were photochemically  
37 generated using  $[\text{Ru}(\text{bpy-OMe})_3]^{2+}$  as a chromophore, BIH as a reductive quencher, and TEOA as a base.  
38 The excited state of  $[\text{Ru}(\text{bpy-OMe})_3]^{2+}$  oxidizes the BIH donor, producing a strong reductant,  $[\text{Ru}(\text{bpy-}$   
39  $\text{OMe})_3]^+$ , and a radical cation,  $\text{BIH}^+$ . The redox chemistry and sacrificial behavior of the electron donor,  
40 BIH, requires a base to deprotonate  $\text{BIH}^+$  to the  $\text{BI}^\bullet$  radical (Scheme 1).<sup>36</sup> This radical intermediate is a  
41 potent reductant ( $E_{1/2} = -1.43$  V vs NHE; or  $-2.06$  V vs  $\text{Fc}^{+/0}$ ),<sup>37</sup> capable of reducing either the  
42 chromophore or the catalyst in the dark. The final  $\text{BI}^+$  oxidized form does not take part in regeneration  
43 reactions. Once the singly-reduced  $[\text{Ru}(\text{bpy-OMe})_3]^+$  is formed, it may transfer an electron to the catalyst,  
44 which is the subject of interest here. The electron transfer steps are diffusion-controlled bimolecular  
45  
46  
47  
48  
49  
50  
51  
52  
53  
54  
55  
56  
57  
58  
59  
60

reactions<sup>36</sup> and are not the focus of this work. Instead, we investigated the chemical transformations of the catalyst after being reduced by one electron.

Scheme 1. Redox chemistry and acidity of BIH in CH<sub>3</sub>CN. Potentials are vs. NHE.



All time-resolved experiments were performed with 0.5 mM [Ru(bpy-OMe)<sub>3</sub>]<sup>2+</sup>, 5 mM Ru(CO)(X)<sup>n+</sup>, and 0.2 M BIH in either neat CH<sub>3</sub>CN or 1.4 M TEOA/CH<sub>3</sub>CN solution, saturated with either N<sub>2</sub> or CO<sub>2</sub>. Under these conditions, the electron transfer to Ru(CO)(X)<sup>n+</sup> is complete in a few hundred nanoseconds (250 – 750 ns). In the absence of a base, BIH<sup>•+</sup> is a reversible quencher and charge recombination between the singly-reduced Ru(CO)(X)<sup>n-1</sup> and BIH<sup>•+</sup> follows second-order equal concentration kinetics. For all Ru(CO)(X)<sup>n+</sup> complexes studied, charge recombination occurs on the microsecond timescale with rate constants, *k*<sub>cr</sub>, ranging from 0.4 – 2 × 10<sup>10</sup> M<sup>-1</sup> s<sup>-1</sup>, with no net photochemistry (Figure S8).

TEOA itself is a common sacrificial electron donor.<sup>3</sup> However, in cases where a chromophore requires a more potent reductant, such as BIH, TEOA is added to the solution solely to act as a Brønsted base, with the assumption that it will ensure deprotonation of the oxidized radical, BIH<sup>•+</sup> (Scheme 1). This prevailing belief was initially assumed by us. However, our transient data revealed that TEOA is extremely inefficient at deprotonating BIH<sup>•+</sup> in CH<sub>3</sub>CN. Thus, photochemical reduction of the Ru(CO)(X)<sup>n+</sup> complexes in 1.4 M TEOA/CH<sub>3</sub>CN solution did not result in persistent, irreversible, absorption changes. Instead, a large fraction (~90%) of the transients generated after pulsed laser excitation undergo unproductive charge recombination with BIH<sup>•+</sup>. For Ru(CO)(CO-TEOA)<sup>+</sup>, Ru(CO)(HCOO)<sup>+</sup>, and Ru(CO)(COOH)<sup>+</sup>, the absorption changes were complex and will be examined shortly. For Ru(CO)(CH<sub>3</sub>CN)<sup>2+</sup>, the ν(CO) transient absorption band displayed a 40 cm<sup>-1</sup> shift to lower energy consistent with one-electron reduction, i.e. Ru(CO)(CH<sub>3</sub>CN)<sup>2+</sup> + e<sup>-</sup> → Ru(CO)(CH<sub>3</sub>CN)<sup>+</sup> (Figure S9). Kinetic traces that report on the concentration profile of Ru(CO)(CH<sub>3</sub>CN)<sup>+</sup> in the presence of TEOA did not follow second-order equal concentration kinetics, while a small, ~10%, fraction of Ru(CO)(CH<sub>3</sub>CN)<sup>+</sup> was still present at longer timescales. The kinetic traces were instead well modeled by a set of two rate equations that coupled the time-dependent concentration of Ru(CO)(CH<sub>3</sub>CN)<sup>+</sup> with the slow deprotonation of BIH<sup>•+</sup> by TEOA (Equations 1–2),

$$\frac{d[Ru^+]}{dt} = -k_{cr}[Ru^+][BIH^{*+}] \quad 1$$

$$\frac{d[BIH^{*+}]}{dt} = -k_{cr}[Ru^+][BIH^{*+}] - k_{dp}[TEOA][BIH^{*+}] \quad 2$$

where  $k_{cr}$  is the second-order rate constant for charge recombination and  $k_{dp}$  is the rate constant for deprotonation of  $BIH^{*+}$ . In a 1.4 M TEOA/ $CH_3CN$  solution containing 0.2 M BIH, the numerical solution of equations 1-2 to the  $Ru(CO)(CH_3CN)^+$  kinetic trace (Figure S9c) provided  $k_{dp} = 4.5 \times 10^3 \text{ M}^{-1} \text{ s}^{-1}$ . This result shows that the deprotonation of  $BIH^{*+}$  by TEOA is slow and therefore, insufficient to kinetically compete with charge recombination. Similar results were obtained for  $Ru(CO)(H)^+$  under the same conditions.

The quantitative deprotonation of  $BIH^{*+}$  in the absence of competitive redox chemistry is an acid-base chemical reaction that requires a proton acceptor that is at least 2  $pK_a$  units more basic than the  $pK_a$  of  $BIH^{*+}$ . The  $pK_a$  of  $BIH^{*+}$  was estimated to be 14.4, from thermodynamic relationships using available values for hydricity and reduction potentials in  $CH_3CN$  (see SI).<sup>37-38</sup> The nitrogen acidity of the conjugate acid of TEOA ( $TEOAH^+$ ) in  $CH_3CN$  has been estimated using calorimetric methods,  $pK_a^N = 15.9$ .<sup>39</sup> Here,  $pK_a^N = 13.74$  was estimated using an isodesmic relationship with the known  $pK_a$  for  $TEAH^+$  (18.82)<sup>39-40</sup> and DFT-computed free energies for the acid-base reaction,  $TEOA(H^+) + TEA \rightleftharpoons TEOA + TEA(H^+)$ . Regardless of the methodology employed to obtain the  $pK_a^N$  of  $TEOAH^+$ , the acid-base equilibrium predicts that 40 – 97% of the  $BIH^{*+}$  should be deprotonated. However, despite favorable thermodynamics, the deprotonation reaction is slow compared with recombination.

The slow deprotonation reaction of  $BIH^{*+}$  by TEOA in  $CH_3CN$  was contrasted with other proton acceptors with known  $pK_a$  values in  $CH_3CN$  (Figure S10): triethylamine ( $pK_a(TEAH^+) = 18.8$ )<sup>39-40</sup>, formate ( $pK_a(HCOOH) = 20.7$ )<sup>41</sup>, and 1,8-diazabicyclo[5.4.0]undec-7-ene ( $pK_a(DBUH^+) = 24.34$ )<sup>40</sup>. The kinetic data obtained from the photochemical reduction of  $Ru(CO)(H)^+$  were analyzed according to numerical solutions to equations 1-2, from which rate constants for the deprotonation of  $BIH^{*+}$  were extracted ( $k_{dp}^{TEA} = 5.5 \times 10^5 \text{ M}^{-1} \text{ s}^{-1}$ ;  $k_{dp}^{HCOO^-} = 7.4 \times 10^6 \text{ M}^{-1} \text{ s}^{-1}$ ;  $k_{dp}^{DBU} = 3.0 \times 10^7 \text{ M}^{-1} \text{ s}^{-1}$ ). When plotted on a logarithmic scale, the obtained rate constants exhibit a linear dependence on the  $pK_a$  of the base, consistent with the predicted behavior of Brønsted acid-base catalyzed reactions. About 1 M TEA was sufficient to induce ~ 90% irreversibility in the photoreduction of the  $Ru(CO)(H)^+$  complex, while the stronger bases  $HCOO^-$  and DBU, only required a few tens of millimolar concentration. Indeed, a recent study has shown that substitution of molar concentrations of TEOA with millimolar levels of DBU, more

than doubled the overall photocatalytic performance for the reduction of  $\text{CO}_2$  to  $\text{CO}$  with rhenium-tricarbonyl type catalysts.<sup>42</sup>

The photochemical one-electron reductions of  $\text{Ru}(\text{CO})(\text{CO})^{2+}$ ,  $\text{Ru}(\text{CO})(\text{HCOO})^+$ , and  $\text{Ru}(\text{CO})(\text{H})^+$  obtained in neat  $\text{CH}_3\text{CN}$  and 1.4 M TEOA/ $\text{CH}_3\text{CN}$  solutions, will be examined in the following sections.

**TRIR of  $\text{Ru}(\text{CO})(\text{CO})^{2+}$ .** Photochemical reduction of  $\text{Ru}(\text{CO})(\text{CO})^{2+}$  in  $\text{CH}_3\text{CN}$  in the presence of BIH but in the absence of TEOA resulted in a bleach of the carbonyl vibration bands at 2096 and 2040  $\text{cm}^{-1}$  and the formation of two new  $\nu(\text{CO})$  bands at 2067 and 2008  $\text{cm}^{-1}$  (Figure 5a). This was expected, considering that the ligand-based reduction increases the  $\pi$ -donation from the metal to the carbonyl ligands. While the irreversible two-electron reduction of  $\text{Ru}(\text{CO})(\text{CO})^{2+}$  was reported to cause CO-ligand loss from electrochemical measurements in solution,<sup>8</sup> or cause the loss of a bipyridine ligand to form polymeric structures,<sup>43</sup> it is unclear from CV data whether such labilization occurs at the first, or second discrete one-electron reduction due to the irreversible nature and closely spaced redox potentials.<sup>2</sup> According to the data shown in Figures 5a and S8a, reversible recombination of the singly-reduced  $\text{Ru}(\text{CO})(\text{CO})^+$  with  $\text{BIH}^{+\bullet}$  occurred in a few tens of microseconds with no net photochemistry involving dissociation of CO.

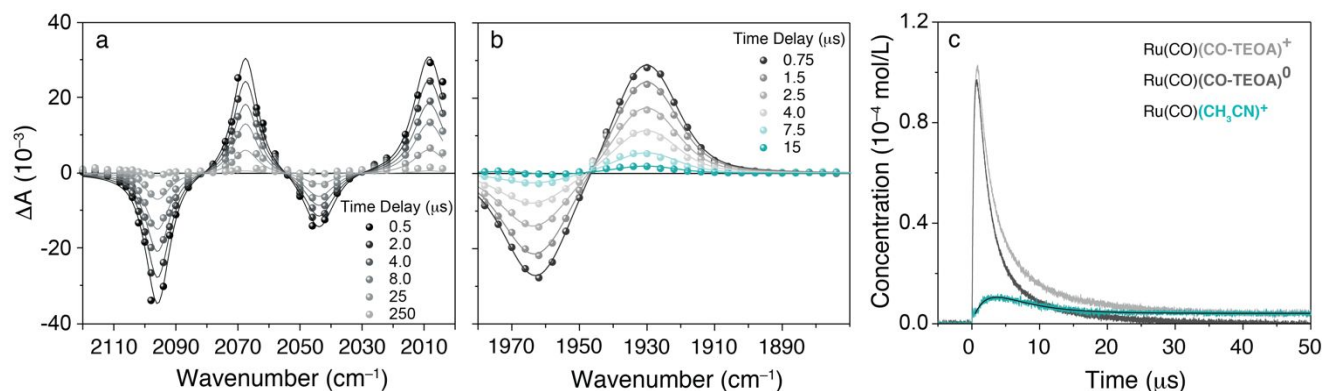
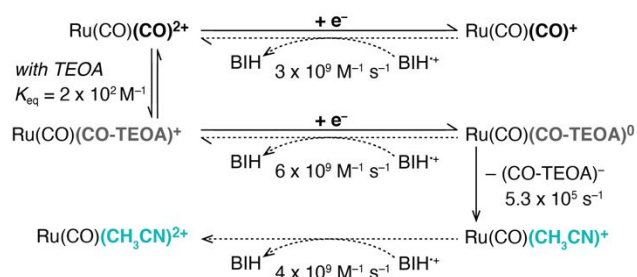


Figure 5. TRIR spectra of (a)  $\text{Ru}(\text{CO})(\text{CO})^{2+}$  in neat  $\text{CH}_3\text{CN}$  and (b)  $\text{Ru}(\text{CO})(\text{CO-TEOA})^+$  in 1.4 M TEOA/ $\text{CH}_3\text{CN}$ , measured at the indicated time delays after pulsed 532 nm excitation of the  $[\text{Ru}(\text{bpy-OMe})_3]^{2+}$  chromophore in the presence of 0.2 M BIH. Overlaid are spectral simulations based on a least squares fit of known  $\nu(\text{CO})$  IR spectra. (c) Simulated time-dependent concentration profiles of the transient species present in (b) based on a least squares fit global analysis. The trace for  $\text{Ru}(\text{CO})(\text{CO-TEOA})^+$  represents how much of the starting material is depleted as a function of time.

In 1.4 M TEOA/ $\text{CH}_3\text{CN}$ , the equilibrated form of  $\text{Ru}(\text{CO})(\text{CO})^{2+}$  is  $\text{Ru}(\text{CO})(\text{CO-TEOA})^+$ , with a single  $\nu(\text{CO})$  vibration at 1962  $\text{cm}^{-1}$ . Photochemical reduction of  $\text{Ru}(\text{CO})(\text{CO-TEOA})^+$  resulted in absorption changes at early timescales consistent with the bleach of this single  $\nu(\text{CO})$  vibration concurrent

with the appearance of a new absorption band at  $1928\text{ cm}^{-1}$  assigned to the  $\nu(\text{CO})$  of the singly-reduced  $\text{Ru}(\text{CO})(\text{CO-TEOA})^0$  (Figure 5b). At time scales beyond  $5\ \mu\text{s}$  the absorptions were not unique to  $\text{Ru}(\text{CO})(\text{CO-TEOA})^{+/0}$ , but instead indicated the coexistence of additional intermediates. The spectra were satisfactorily modeled by a least squares fit of the known IR spectra of the *bleached*- $\text{Ru}(\text{CO})(\text{CO-TEOA})^+$ , singly-reduced  $\text{Ru}(\text{CO})(\text{CO-TEOA})^0$  and  $\text{Ru}(\text{CO})(\text{CH}_3\text{CN})^+$  (Figure S11). Analysis of the deconvoluted concentration profiles revealed that the singly-reduced *solvento* complex,  $\text{Ru}(\text{CO})(\text{CH}_3\text{CN})^+$ , is partially formed in kinetic competition with charge recombination. Since the rate at which  $\text{Ru}(\text{CO})(\text{CH}_3\text{CN})^+$  is formed,  $k = 5.3 \times 10^5\text{ s}^{-1}$ , must coincide with that of the loss of the  $(\text{CO-TEOA})^-$  ligand, the overall ligand exchange reaction,  $\text{Ru}(\text{CO})(\text{CO-TEOA})^0 + \text{CH}_3\text{CN} \rightarrow \text{Ru}(\text{CO})(\text{CH}_3\text{CN})^+ + (\text{CO-TEOA})^-$  is a clear indication of *CO dissociation assisted by TEOA*. An overview of the reactions involved in the photochemical one-electron reduction of  $\text{Ru}(\text{CO})(\text{CO})^{2+}$  and  $\text{Ru}(\text{CO})(\text{CO-TEOA})^+$  is shown in Scheme 2.1.

Scheme 2.1



**TRIR of  $\text{Ru}(\text{CO})(\text{HCOO})^+$ .** The photochemical reduction of  $\text{Ru}(\text{CO})(\text{HCOO})^+$  in neat  $\text{CH}_3\text{CN}$  solution resulted in a  $\nu(\text{CO})$  vibration that was  $38\text{ cm}^{-1}$  shifted to lower energy, with a clean isosbestic point around  $1960\text{ cm}^{-1}$  (Figure 6a). Consistent with data obtained from spectroelectrochemical experiments, the new band centered at  $1938\text{ cm}^{-1}$  was assigned to the  $\nu(\text{CO})$  vibration of the singly-reduced *formato* complex,  $\text{Ru}(\text{CO})(\text{HCOO})^0$ . There was no net photochemistry involving the loss of  $\text{HCOO}^-$  or  $\text{CO}$  on the timescale of charge recombination. Persistent photochemical reduction of  $\text{Ru}(\text{CO})(\text{HCOO})^+$  was obtained by adding  $50\text{ mM}$  TBAHCOO as a base to the  $\text{CH}_3\text{CN}$  solution (Figure S12b-c). Although the presence of formate salt may alter the equilibrium and rates that connect reactants and products in  $\text{Ru}(\text{CO})(\text{HCOO})^0 + \text{CH}_3\text{CN} \rightleftharpoons \text{Ru}(\text{CO})(\text{CH}_3\text{CN})^+ + \text{HCOO}^-$ , there was no evidence for the loss of formate since the concentration of  $\text{Ru}(\text{CO})(\text{HCOO})^0$  initially formed remained unchanged on the millisecond timescale.

The TRIR spectra recorded in 1.4 M TEOA/CH<sub>3</sub>CN are shown in Figure 6b. Immediately after the reduction of Ru(CO)(HCOO)<sup>+</sup>, the singly-reduced Ru(CO)(HCOO)<sup>0</sup> was formed. From this point forward, the absorption changes were complex implying the coexistence of multiple transient species. The spectral and kinetic data were adequately modeled with a weighted sum of known IR spectra of the *bleached*-Ru(CO)(HCOO)<sup>+</sup>, Ru(CO)(HCOO)<sup>0</sup> and Ru(CO)(CH<sub>3</sub>CN)<sup>+</sup>. Quantitative analysis of the time-dependent concentration profiles revealed that Ru(CO)(CH<sub>3</sub>CN)<sup>+</sup> is partially formed in kinetic competition with charge recombination, and must coincide with the rate of the formate ion dissociation ( $5.5 \times 10^5 \text{ s}^{-1}$ ). Thus, analogously to the electrochemical data in the presence of TEOA, the photochemically-generated singly-reduced Ru(CO)(HCOO)<sup>0</sup> undergoes accelerated dissociation of formate product in the presence of TEOA. An overview of these reactions in the presence and absence of TEOA is shown in Scheme 2.2.

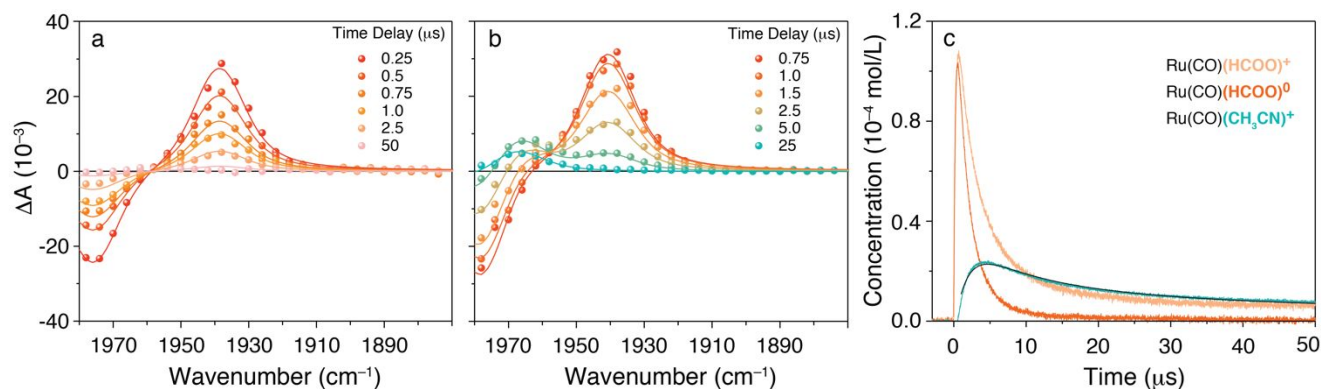
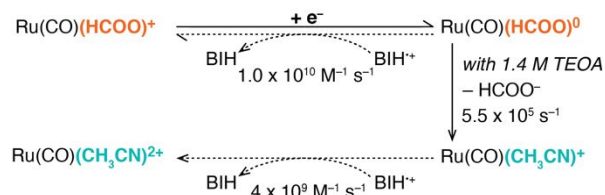


Figure 6. TRIR spectra of Ru(CO)(HCOO)<sup>+</sup> measured at the indicated time delays after pulsed 532 nm excitation of the [Ru(bpy-OMe)<sub>3</sub>]<sup>2+</sup> chromophore in the presence of 0.2 M BIH: (a) in neat CH<sub>3</sub>CN and (b) in 1.4 M TEOA/CH<sub>3</sub>CN. Overlaid are spectral simulations based on a least squares fit of known  $\nu(\text{CO})$  IR spectra. (c) Simulated time-dependent concentration profiles of the transient species present in (b) based on a least squares fit global analysis. The trace for Ru(CO)(HCOO)<sup>+</sup> represents how much of the starting material is depleted as a function of time.

#### Scheme 2.2.



**TRIR of Ru(CO)(H)<sup>+</sup>.** Similar to all previous measurements performed in neat CH<sub>3</sub>CN solution, the TRIR spectra recorded for Ru(CO)(H)<sup>+</sup> were characteristic of the reversible reduction to Ru(CO)(H)<sup>0</sup> (Figure

7a). The  $\text{Ru}(\text{CO})(\text{H})^+$  bleach was centered at  $1930\text{ cm}^{-1}$  and a lower energy  $\nu(\text{CO})$  band at  $1894\text{ cm}^{-1}$  that was assigned to the singly-reduced hydrido complex,  $\text{Ru}(\text{CO})(\text{H})^0$ , appeared. Experiments performed in saturated  $\text{CO}_2$  (0.28 M), did not result in the expected hydride transfer reactivity to  $\text{CO}_2$  during the timescale of charge recombination. As described earlier in this section, the addition of 50 mM of TBAHCOO as a base was sufficient to irreversibly generate  $\text{Ru}(\text{CO})(\text{H})^0$  in  $\text{N}_2$ -saturated solution (Figure S13a-b). Kinetic traces monitored at  $1894\text{ cm}^{-1}$  were recorded as a function of known titrated amounts of  $\text{CO}_2$ , Figure S13c-d. All kinetic traces displayed monoexponential behavior, and according to the rate law equation written for the metal-hydride reactivity with  $\text{CO}_2$ , equation 3, they were indicative of a pseudo-first-order kinetic reaction.

$$\frac{d[\text{Ru}(\text{CO})(\text{H})^0]}{dt} = -k_{\text{HT}}[\text{CO}_2][\text{Ru}(\text{CO})(\text{H})^0] \quad 3$$

Quantitative analysis of these data provided a rate constant for hydride transfer to  $\text{CO}_2$  of  $k_{\text{HT}} = 9.6\text{ M}^{-1}\text{ s}^{-1}$  to produce the singly-reduced *formato* complex,  $\text{Ru}(\text{CO})(\text{HCOO})^0$ .

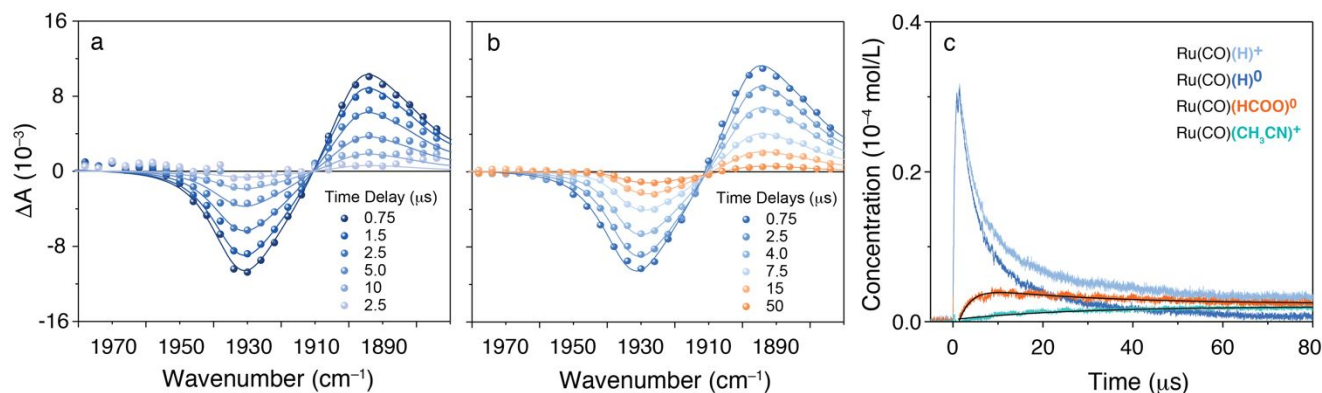
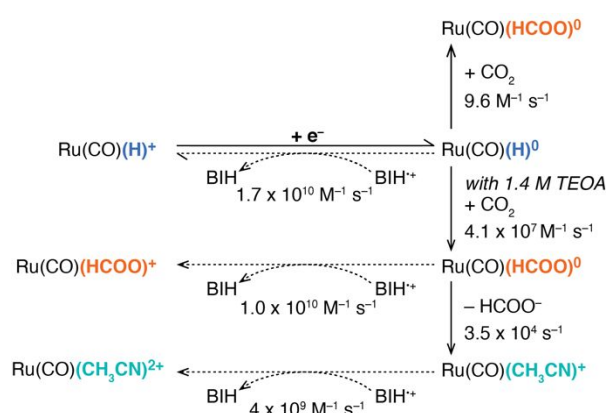


Figure 7. TRIR spectra of  $\text{Ru}(\text{CO})(\text{H})^+$  measured at the indicated time delays after pulsed 532 nm excitation of the  $[\text{Ru}(\text{bpy-OMe})_3]^{2+}$  chromophore in the presence of 0.2 M BIH: (a) in neat  $\text{CH}_3\text{CN}$  and (b) in 0.7 M TEOA/ $\text{CH}_3\text{CN}$ . Overlaid are spectral simulations based on a least squares fit of known  $\nu(\text{CO})$  IR spectra. (c) Simulated time-dependent concentration profiles of the transient species present in (b) based on a least squares fit global analysis. The trace for  $\text{Ru}(\text{CO})(\text{H})^+$  represents how much of the starting material is depleted as a function of time.

TRIR measurements on the photochemical reduction of  $\text{Ru}(\text{CO})(\text{H})^+$  in the presence of TEOA showed unexpected complications. A slow but gradual formation of  $\text{Ru}(\text{CO})(\text{HCOO})^+$  was observed during the sample preparation in the  $\text{CO}_2$  saturation step prior to the transient measurement. This complicates the analysis of hydride transfer to  $\text{CO}_2$  because direct reduction of the existing  $\text{Ru}(\text{CO})(\text{HCOO})^+$  can result in misinterpretation of the data. In order to minimize such undesired reactivity prior to the experiment, a

solution containing the catalyst was mixed with a second solution containing only CO<sub>2</sub> (0.28 M) immediately before pulsed laser excitation using syringe pumps and gas-tight syringes. The solutions were mixed with equal volumes such that the final concentration of CO<sub>2</sub> was (0.14 M). It is worth noting that the zwitterionic capture of CO<sub>2</sub> by TEOA under these conditions resulted in a 10 mM concentration of CO<sub>2</sub>-TEOA. The TRIR spectra measured for Ru(CO)(H)<sup>+</sup> were recorded with a fresh aliquot every 2–3 data points. The absorption changes that follow the photochemical one-electron reduction of Ru(CO)(H)<sup>+</sup> showed an apparent time-dependent red-shift of the bleach at 1930 cm<sup>-1</sup> concurrent with the decay of the Ru(CO)(H)<sup>0</sup> absorbance at 1894 cm<sup>-1</sup> (Figure 7b).

Scheme 2.3.



A careful global analysis of the data (Figure 7c), revealed that the singly-reduced *formato* complex was formed at an observed rate of 4.1 × 10<sup>5</sup> s<sup>-1</sup>, after which it slowly decayed to reach an equilibrium concentration with the formation of the singly-reduced *solvento* complex, Ru(CO)(CH<sub>3</sub>CN)<sup>+</sup>, at a rate of 3.5 × 10<sup>4</sup> s<sup>-1</sup>. A representative example of the overlapped transient species taken at 15 μs after pulsed laser excitation is shown in Figure S14a. Single kinetic traces were also measured at saturation concentrations of CO<sub>2</sub> and CO<sub>2</sub>-TEOA (278 mM and 20 mM, respectively), at wavenumbers that predominantly reported on the concentrations of *bleached*-Ru(CO)(H)<sup>+</sup>, Ru(CO)(H)<sup>0</sup>, Ru(CO)(HCOO)<sup>0</sup>, and Ru(CO)(CH<sub>3</sub>CN)<sup>+</sup>, Figure S14b. The overall absorption changes were identical to those shown in Figure 7c, but the rate (8.2 × 10<sup>5</sup> s<sup>-1</sup>), and amplitude of Ru(CO)(HCOO)<sup>0</sup> formation increased. This result demonstrates a CO<sub>2</sub> concentration effect on the formation of the singly-reduced *formato* complex, from which tentative plots of the obtained rates as a function of the CO<sub>2</sub> and CO<sub>2</sub>-TEOA concentrations provided rate constants for hydride transfer in the presence of TEOA to CO<sub>2</sub> and CO<sub>2</sub>-TEOA of  $k_{HT} = 2.8 \times 10^6 \text{ M}^{-1} \text{ s}^{-1}$  and  $k_{HT} = 4.1 \times 10^7 \text{ M}^{-1} \text{ s}^{-1}$ , respectively (Figure S14c-d). These rate constants are about 5–6 orders of magnitude larger

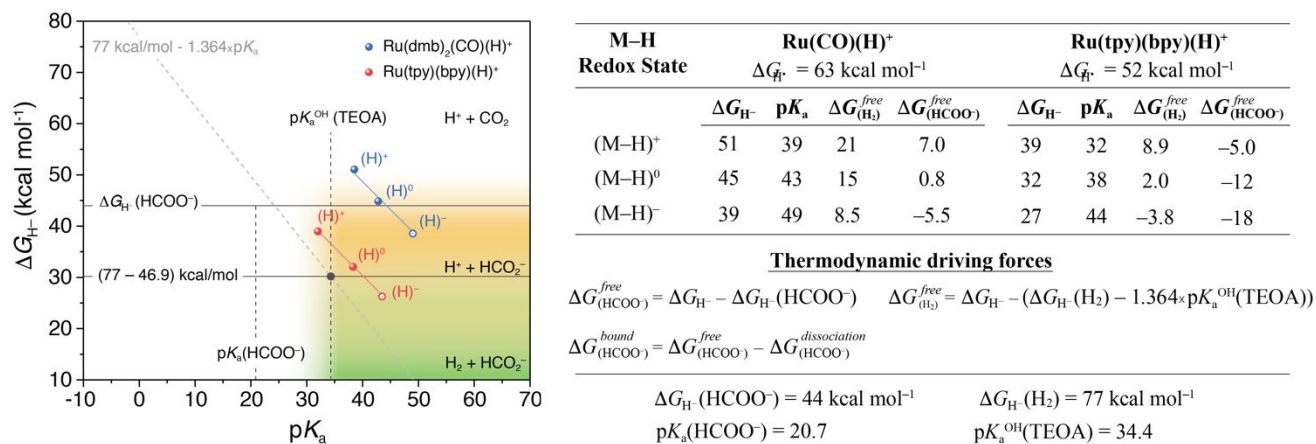
1  
2  
3 than those measured for the hydride transfer to CO<sub>2</sub> in CH<sub>3</sub>CN solutions without TEOA, and the  
4 implications of this result to the catalytic reduction of CO<sub>2</sub> to formate will be more rigorously examined  
5 in the Discussion section. An overview of the reactions involved in the photochemical one-electron  
6 reduction of Ru(CO)(H)<sup>+</sup> in the presence and absence of TEOA is shown in Scheme 2.3.  
7  
8  
9

## 10 11 **DISCUSSION**

12  
13 While decades of research has promoted the design of a large number of CO<sub>2</sub> reduction catalysts, most  
14 studies focus on the *macro-observations* of product selectivity and catalyst performance. More rigorous  
15 examination of the catalytic pathways is often conducted using electrochemical and computational  
16 methods, while only a limited number of studies succeeded in identifying transient intermediates, their  
17 kinetics and contributions to the overall catalytic reaction. In this discussion, the electrochemical and  
18 spectroscopic data presented earlier will be combined to provide a global view of the thermodynamics and  
19 kinetic events in the reduction of CO<sub>2</sub> to formate by Ru(II)-carbonyl catalysts. This includes the key steps  
20 of formate ion dissociation, metal hydride formation and the hydride transfer to CO<sub>2</sub> to produce the metal-  
21 bound formate intermediate. Complementary DFT calculations were guided by the experimental results  
22 to provide a comparative interpretation of the free energy landscape of the relevant catalytic steps. While  
23 TEOA is customarily used in most photochemical assays, its active participation in the catalytic pathways  
24 is often disregarded. Here, this concern will be brought into context for discussion. Though there has been  
25 early work,<sup>2, 8</sup> and some recent indications,<sup>44</sup> that suggest a connection between metal-formate and  
26 metalcarboxylic acid intermediates, the results discussed here will examine the metal hydride,  
27 Ru(CO)(H)<sup>+</sup>, as the active catalyst and its ability to reduce CO<sub>2</sub>.  
28  
29  
30  
31  
32  
33  
34  
35  
36  
37  
38

39  
40 ***Thermodynamic considerations.*** Hydricity is a thermodynamic measure of the Gibbs free energy change,  
41  $\Delta G_{\text{H}^-}^{\circ}$ , for the heterolytic dissociation of the metal-hydride bond, and is conceptually used to quantify the  
42 ability of a metal hydride to donate a hydride ion. Since the catalytic production of H<sub>2</sub> and formate are  
43 intimately connected to metal hydride intermediates, a proper knowledge of the thermodynamic hydricity  
44 allows for a predictive estimate of product selectivity. Here, the competitive hydride reactivity for the  
45 reduction of H<sup>+</sup> and CO<sub>2</sub> are illustrated in Scheme 3, where the thermodynamic hydricity and pK<sub>a</sub> of the  
46 reaction components are combined in a diagram that allows for direct and quantitative analysis of the  
47 overall reaction driving forces.<sup>45</sup> Once the pK<sub>a</sub> of the proton source is defined, the diagram establishes  
48 specific thermodynamic boundaries that regulate product selectivity and limit the choices of metal  
49 hydrides that can operate under catalytic conditions.  
50  
51  
52  
53  
54  
55  
56  
57  
58  
59  
60

The hydricity of formate,  $\Delta G_{\text{H}^-}^{\circ}(\text{HCOO}^-) = 44 \text{ kcal mol}^{-1}$  in  $\text{CH}_3\text{CN}$ ,<sup>46</sup> imposes an upper limit for exergonic reactions of metal hydrides to reduce  $\text{CO}_2$  to formate. Theoretically, the more hydridic the metal hydride, the more facile the hydride transfer to  $\text{CO}_2$  becomes. This is reasonably true for stoichiometric reactions in the absence of proton sources. For a metal hydride to become catalytic, protons are necessary to reform the metal hydride at the end of the catalytic cycle, and this requirement introduces thermodynamic boundaries that may constrain its catalytic activity. In this context, the  $\text{p}K_{\text{a}}$  of the proton source becomes a delimiter for the metal hydride recycling, while at the same time it establishes the driving force for  $\text{H}_2$  evolution,  $\Delta G_{\text{H}_2} = \Delta G_{\text{H}^-} - (\Delta G_{\text{H}^-}(\text{H}_2) - 1.364 \times \text{p}K_{\text{a}})$ , where  $\Delta G_{\text{H}^-}$  is the hydricity of a metal hydride and  $\Delta G_{\text{H}^-}(\text{H}_2) = 77 \text{ kcal mol}^{-1}$  is a measure of the free energy of dissociation of  $\text{H}_2$  to form a hydride ion and free proton in  $\text{CH}_3\text{CN}$ .<sup>46</sup> If only the hydride transfer step is considered, one may naturally conclude that the higher the  $\text{p}K_{\text{a}}$  of a proton source, the more difficult  $\text{H}_2$  evolution becomes, and therefore it results in lower competitive catalysis for the reduction of  $\text{CO}_2$  to formate. However, as mentioned earlier, the choice of a proton source must be carefully considered to allow for the protonation of the metal center to reform the active metal hydride complex. An example of these considerations is given in Scheme 3 where the TEOA hydroxy groups act as the proton source.



Scheme 3. Free energy relationships for metal hydride reactivity to produce formate and/or  $\text{H}_2$ . The indicated  $\text{p}K_{\text{a}}$  of the TEOA hydroxy groups limits the cyclability of the metal hydride and defines the driving force for  $\text{H}_2$  evolution. Hydricity and  $\text{p}K_{\text{a}}$  values for  $[\text{Ru}(\text{dmb})_2(\text{CO})(\text{H})]^+$  and  $[\text{Ru}(\text{tpy})(\text{bpy})(\text{H})]^+$  are compared for discussion. All values are reported with two significant digits (see SI).

For reasons that will be clarified later, TEOA is considered here as a proton source and the estimated acidity for its hydroxy groups ( $\text{p}K_{\text{a}}^{\text{OH}} = 34.4$ ) was used to complete the diagram in Scheme 3. Calculated hydricity values for two metal hydrides,  $[\text{Ru}(\text{dmb})_2(\text{CO})(\text{H})]^+$  and  $[\text{Ru}(\text{tpy})(\text{bpy})(\text{H})]^+$ , at three different redox states were combined with their related  $\text{p}K_{\text{a}}$  values and included in the diagram for discussion. The

1  
2  
3 reaction driving forces for hydride transfer to  $H^+$  and  $CO_2$  were quantified according to known free energy  
4 relationships shown in Scheme 3.<sup>45</sup> The hydricity value for  $[Ru(dmb)_2(CO)(H)]^+$  was experimentally  
5 determined as  $\Delta G_{H^-} = 51 \pm 0.5 \text{ kcal mol}^{-1}$  by means of direct hydride transfer and by the  $H_2$  heterolysis  
6 method.<sup>46-47</sup> Complementary DFT computational methods provided an estimated hydricity value of  $\Delta G_{H^-}$   
7 =  $50.8 \text{ kcal mol}^{-1}$  using an isodesmic relationship, which is in good agreement with the experimental  
8 data.<sup>48</sup> Additional hydricity values for different redox states of the metal hydrides, the homolytic bond  
9 cleavage of a metal-hydride bond and  $pK_a$  values were determined according to free energy relationships  
10 described by known thermochemical cycles.<sup>45-46, 49</sup> Details on the methodologies employed are described  
11 in the SI.  
12  
13  
14  
15  
16  
17  
18

19  
20 The hydricity of  $Ru(tpy)(bpy)(H)^+$  is sufficient to exergonically reduce  $CO_2$  to the formate anion  
21 without additional reduction of the catalyst with  $\Delta G_{(HCOO^-)} = -5.0 \text{ kcal mol}^{-1}$ , while this same reaction is  
22  $7.0 \text{ kcal mol}^{-1}$  endergonic for  $Ru(CO)(H)^+$ . In cases where it is necessary to enhance the reactivity of  
23 metal hydrides, ligand- or metal-based reductions have widely been employed as a means to increase  
24 electron density at the metal hydride bond.<sup>11, 46</sup> For instance, the singly-reduced forms of the metal  
25 hydrides listed here become  $\sim 6.5 \text{ kcal mol}^{-1}$  more hydridic compared to their initial resting state.  
26 Additional ligand-based reductions monotonically enhance the reactivity of metal hydrides towards the  
27 reduction of  $CO_2$ , though it may collaterally increase the susceptibility to competitive  $H_2$  evolution.  
28 Although  $[Ru(tpy)(bpy)(H)]^+$  is a better hydride donor than  $Ru(CO)(H)^+$  and  $Ru(CO)(H)^0$ , the  
29 thermodynamic boundaries imposed by TEOA as the proton source impede the metal hydride to be  
30 reformed under catalytic conditions given that the TEOA hydroxy groups are more basic than  
31  $[Ru(tpy)(bpy)(H)]^+$ .  
32  
33  
34  
35  
36  
37  
38  
39  
40

41 Activation of  $Ru(CO)(H)^+$  to the more hydridic singly-reduced  $Ru(CO)(H)^0$  is necessary to achieve  
42 more favorable thermodynamic driving forces for formate anion production, with  $\Delta G_{(HCOO^-)} = 0.8 \text{ kcal}$   
43  $\text{mol}^{-1}$ , while still being incompetent for  $H_2$  evolution,  $\Delta G_{(H_2)} = 15 \text{ kcal mol}^{-1}$ . Besides, the strong basicity  
44 of  $Ru(CO)(H)^+$  allows for the use of proton sources with  $pK_a$  values as high as 39, thus making hydrogen  
45 evolution even more difficult, while allowing for  $Ru(CO)(H)^+$  to be re-formed. The increased hydricity of  
46 the doubly-reduced  $Ru(CO)(H)^-$  facilitates hydride transfer to  $CO_2$ ,  $\Delta G_{(HCOO^-)} = -5.5 \text{ kcal mol}^{-1}$ , with  
47 predominant selectivity over  $H_2$  evolution,  $\Delta G_{(H_2)} = 8.5 \text{ kcal mol}^{-1}$  with TEOA as the proton source,  
48 although at the cost of an additional 0.2 V for activation.  
49  
50  
51  
52  
53  
54  
55  
56  
57  
58  
59  
60

1  
2  
3 One must emphasize that despite the relations derived from Scheme 3 providing predictions for  
4 reaction equilibria, they are purely thermodynamic and do not account for the kinetic aspects of the  
5 reaction activation barriers, which may decisively control the final outcomes in catalytic reactions that  
6 have multiple competitive pathways.<sup>45</sup> Additionally, these relationships consider the overall reactions with  
7 HCOO<sup>-</sup> and H<sub>2</sub> as final products, yet most intermediate products that follow from a hydride transfer step  
8 exist transiently coordinated to the metal center as M–HCOO<sup>-</sup> or M–H<sub>2</sub>. Therefore, additional free energy  
9 corrections that account for this bond cleavage must be considered in order to more accurately report on  
10 reaction driving forces.

11  
12 ***Metal-hydride formation.*** Transition metal hydrides are undeniably recognized as key intermediates in  
13 the conversion of protons to hydrogen gas or CO<sub>2</sub> to formate. It is therefore important to consider here the  
14 circumstances in which they are formed. In most molecular artificial photosynthetic designs for H<sub>2</sub>  
15 evolution and the reduction of CO<sub>2</sub>, protons and electrons are used to source the metal-hydride formation,  
16 provided that the metal has an available coordination site and appropriate pK<sub>a</sub> to allow for protonation.

17  
18 The calculated pK<sub>a</sub> for Ru(CO)(H)<sup>+</sup> (pK<sub>a</sub> = 39) translates into a conjugate base, Ru(CO)(CH<sub>3</sub>CN)<sup>0</sup>,  
19 that is possibly sufficiently basic to deprotonate water (pK<sub>a</sub> = 38 – 41)<sup>46, 50</sup> present in CH<sub>3</sub>CN solutions as  
20 a proton source. In dry CH<sub>3</sub>CN conditions, reductive cyclic voltammetry experiments on  
21 Ru(CO)(CH<sub>3</sub>CN)<sup>2+</sup> and Ru(CO)(HCOO)<sup>+</sup> at 100 mV/s led to ligand loss chemistry and formation of the  
22 unsaturated 5-coordinate Ru(CO)<sup>0</sup>, with no clear electrochemical evidence that Ru(CO)(H)<sup>+</sup> has been  
23 generated. Although this observation may, at first, seem to contradict the results obtained from  
24 spectroelectrochemical measurements, where application of potentials at the second electron reduction  
25 resulted in the irreversible formation of Ru(CO)(H)<sup>+</sup>, one needs to recall that the experimental timescales  
26 are notably different. At fixed applied potentials, an equilibrium amount of Ru(CO)<sup>0</sup> may react with traces  
27 of water and form Ru(CO)(H)<sup>+</sup>. Alternatively, it has been reported that ammonium salts are susceptible to  
28 fragmentation reactions in the presence of strong bases,<sup>51</sup> and this degradation pathway may supply  
29 protons for the protonation of the metal. While precautions were taken to ensure that all experiments were  
30 performed under the driest possible conditions, the formation of Ru(CO)(H)<sup>+</sup> was always observed and  
31 the possibility of residual water as the proton source cannot be ruled out.

32  
33 Ru(CO)(H)<sup>+</sup> metal hydride formation became more evident with the addition of TEOA. Photochemical  
34 assays of CO<sub>2</sub> reduction using molecular catalysts are generally conducted in the presence of high  
35 concentrations of TEOA (1 – 1.4 M), yet much attention is given to the sacrificial quenchers, e.g. BNAH

1  
2  
3 and BIH, as the proton sources once oxidized by one electron. Cyclic voltammetry experiments conducted  
4 in N<sub>2</sub>-saturated 1.4 M TEOA/CH<sub>3</sub>CN solutions exhibited a reduction wave at more negative potentials  
5 that was common to all Ru(CO)(X)<sup>n+</sup> complexes, and which matched the peak potentials for the  
6 Ru(CO)(H)<sup>+0</sup> redox couple. Spectroelectrochemical measurements at potentials just negative enough to  
7 initiate the second reduction of each complex unarguably validated the formation of Ru(CO)(H)<sup>+</sup> as  
8 probed by its characteristic  $\nu(\text{CO})$  stretching vibration at 1930 cm<sup>-1</sup>.  
9

10  
11  
12  
13  
14 The pK<sub>a</sub> of the TEOA hydroxy groups in water (15.12) is comparable to those found for primary  
15 alcohols such as ethanol and methanol (15.5), which is just slightly higher than the pK<sub>a</sub> of water (14).  
16 Although the acidities of alcohols and TEOA have not been experimentally determined in CH<sub>3</sub>CN, they  
17 are expected to behave as weak acids, with pK<sub>a</sub> values as high as those considered for water (pK<sub>a</sub> = 38 –  
18 41)<sup>46, 50</sup>. The ability of the 5-coordinated Ru(CO)<sup>0</sup> complex to abstract a proton from TEOA was tested by  
19 quantifying the free energy associated with the Ru(CO)<sup>0</sup> + TEOA ⇌ Ru(CO)(H)<sup>+</sup> + TEOA(-H<sup>+</sup>) acid-  
20 base reaction using computational methods, from which the TEOA-hydroxy pK<sub>a</sub> of 34.4 was estimated  
21 relative to the calculated value of the Ru(CO)(H)<sup>+</sup> pK<sub>a</sub> of 39. This result supports the experimental  
22 observations that the TEOA-hydroxy groups function as a proton reservoir for the catalytic conversion of  
23 CO<sub>2</sub> to formate, provided that the metal-hydride has the appropriate pK<sub>a</sub>.  
24  
25  
26  
27  
28  
29  
30

31  
32 Organic hydride electron donors, such as BNAH and BIH, have also been considered as proton donors  
33 in photochemical assays when in their oxidized forms, BNAH<sup>•+</sup> and BIH<sup>•+</sup>, since their sacrificial behavior  
34 requires the loss of a proton from their radical cationic form. In this case, two possible protonation  
35 pathways may be considered: 1) the first pathway involves the direct protonation of the metal by BIH<sup>•+</sup>.  
36 The difference in pK<sub>a</sub>'s between BIH<sup>•+</sup> (14.3) and Ru(CO)(H)<sup>+</sup> (39) validates this pathway. However, the  
37 radical cation, BIH<sup>•+</sup> is also an electron acceptor, and thus the direct protonation of the metal from BIH<sup>•+</sup>  
38 is in kinetic competition with unwanted charge recombination reactions; 2) the second pathway uses an  
39 external base functioning as the proton acceptor reservoir, carrier and eventually the proton donor. This  
40 dual character is therefore subject to two prerequisites, i.e., the added base has to be sufficiently basic to  
41 carry out the deprotonation of BIH<sup>•+</sup> but at the same time it must be more acidic than the metal hydride.  
42 Protonated-TEOA, which has a pK<sub>a</sub><sup>N</sup> ~ 14 meets the acidic criterion but, as shown in the Results section,  
43 it inefficiently deprotonates the oxidized BIH<sup>•+</sup> under transient conditions. Notwithstanding that  
44 protonated-TEOA is a better acid than the TEOA-hydroxy groups (pK<sub>a</sub><sup>OH</sup> = 34.4), it is only formed at low  
45 concentrations with kinetics for protonation of the metal that are diffusion-controlled. Therefore, given  
46  
47  
48  
49  
50  
51  
52  
53  
54  
55  
56  
57  
58  
59  
60

1  
2  
3 the experimental evidence that TEOA is capable of sourcing the Ru(CO)(H)<sup>+</sup> metal hydride formation, it  
4 is reasonable to consider TEOA as the predominant proton source in photochemical assays in CH<sub>3</sub>CN.  
5

6  
7 **Hydride transfer.** Computational studies that detail the mechanisms by which CO<sub>2</sub> reacts with metal  
8 hydrides to produce formate are widely more available than experimental investigations.<sup>11, 52-59</sup> This is  
9 largely because of the experimental challenges inherent to the transient detection and short-term stability  
10 of most metal hydrides. Only a few isolated cases in which a metal hydride is capable of reducing CO<sub>2</sub> in  
11 its resting state allowed for more systematic studies.<sup>53-60</sup> The slow reactivity between these metal hydrides  
12 and CO<sub>2</sub> allowed for the time-resolved detection of the hydride transfer step using conventional UV-vis  
13 and NMR spectroscopy or with rapid mixing stopped-flow measurements. The results gathered from these  
14 studies marked the initial steps towards a better understanding of the variables that control the kinetics for  
15 hydride transfer to CO<sub>2</sub>. This includes solvent effects, the presence of Lewis acid additives, and  
16 corroboration of computationally proposed mechanisms.  
17  
18  
19  
20  
21  
22  
23  
24

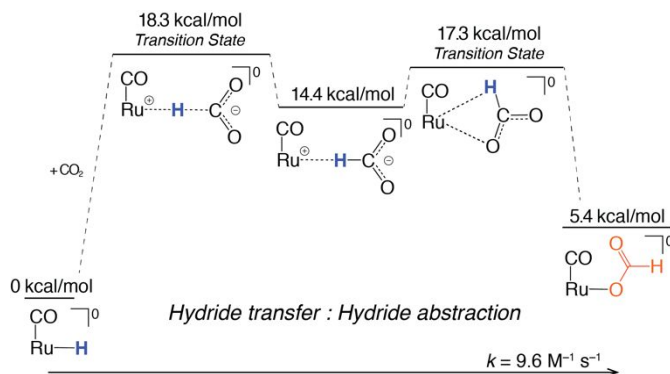
25 To date, the extensive library of computational work has established two prevailing mechanisms for  
26 which a metal hydride may react with CO<sub>2</sub> to produce formate. The first and more frequently  
27 communicated mechanism proposes a stepwise pathway wherein hydride transfer is initiated after the  
28 nucleophilic attack of CO<sub>2</sub> by the metal hydride to form a loosely H-bound formate intermediate – *hydride*  
29 *abstraction*. At this stage, the bound formate may dissociate as the anionic product, or the H-bound  
30 formate may undergo an inner sphere rotational rearrangement that stabilizes the commonly observed O-  
31 bound formate product. The second proposed mechanism introduces the concept of a single concerted  
32 pathway, in which CO<sub>2</sub> inserts into the metal hydride bond to adopt a four-centered intermediate – *CO<sub>2</sub>*  
33 *insertion*.<sup>52, 60</sup> The weak interaction between the CO<sub>2</sub>-oxygen and the metal pulls electron density from  
34 the carbon to break the thermodynamic stability of CO<sub>2</sub>, at the same time as the metal hydride bond is  
35 electron-enriched. This concerted and beneficial interaction ultimately results in facilitated nucleophilic  
36 attack by the metal hydride to form the O-bound formate product. Note that for both mechanistic situations  
37 described, the O-bound formate is the immediate product of the hydride transfer to CO<sub>2</sub>, and as such, the  
38 thermodynamic relationships quantified from Scheme 3,  $\Delta G_{(\text{HCOO}^-)}$ , are not adequate representations of the  
39 real reaction free energy,  $\Delta G_{(\text{HCOO}^-)}^{\text{bound}}$ , for the hydride transfer step. Since a metal-oxygen bond must be  
40 cleaved to afford the final HCOO<sup>-</sup> anion, this free energy must be considered when determining the actual  
41 reaction driving force according to equation 4,  
42  
43  
44  
45  
46  
47  
48  
49  
50  
51  
52  
53

$$\Delta G_{(\text{HCOO}^-)}^{\text{bound}} = \Delta G_{(\text{HCOO}^-)} - \Delta G_{(\text{HCOO}^-)}^{\text{dissociation}} \quad 4$$

1  
2  
3 where  $\Delta G_{(\text{HCOO}^-)}^{\text{dissociation}} = -RT \ln(K_{\text{eq}})$  and  $K_{\text{eq}}$  is the equilibrium constant for formate dissociation (0.03 M),  
4 which was obtained from scan-rate dependent electrochemical data. While the overall free energy change  
5 to generate a  $\text{HCOO}^-$  anion product from reacting the singly-reduced  $[\text{Ru}(\text{dmb})_2(\text{CO})(\text{H})]^0$  with  $\text{CO}_2$  is  $\Delta$   
6  $G_{(\text{HCOO}^-)} = 0.8 \text{ kcal mol}^{-1}$ ,  $\Delta G_{(\text{HCOO}^-)}^{\text{bound}}$  for the hydride transfer step itself is about  $-1.3 \text{ kcal mol}^{-1}$ . A similar  
7 analysis may be considered for  $[\text{Ru}(\text{tpy})(\text{bpy})(\text{H})]^+$  if the equilibrium constant for formate dissociation  
8 from  $[\text{Ru}(\text{tpy})(\text{bpy})(\text{HCOO})]^+$  is known. This value was not measured in the present study, nor was it  
9 available from the literature. Nonetheless, since  $[\text{Ru}(\text{tpy})(\text{bpy})(\text{HCOO})]^+$  is stable and does not  
10 spontaneously dissociate  $\text{HCOO}^-$  without further reduction to  $[\text{Ru}(\text{tpy})(\text{bpy})(\text{HCOO})]^0$ , the reaction free  
11 energy for the hydride transfer step,  $\Delta G_{(\text{HCOO}^-)}^{\text{bound}}$  must be more negative than  $-5.0 \text{ kcal mol}^{-1}$ , given that  $K_{\text{eq}}$   
12 for formate dissociation is a very small number.  
13  
14  
15  
16  
17  
18  
19  
20

21 Here, the reactivity of the  $\text{Ru}(\text{CO})(\text{H})^+$  metal hydride towards  $\text{CO}_2$  is considered and time-resolved in  
22 its transient singly-reduced  $\text{Ru}(\text{CO})(\text{H})^0$  form. To the best of our knowledge, the results disclosed here are  
23 the first ever reported for this class of Ru(II) catalyst and possibly the first to investigate the hydride  
24 transfer to  $\text{CO}_2$  from transiently reduced metal hydride complexes. Guided by the obtained experimental  
25 results, computational methods were utilized to gather further information about the reaction pathways  
26 that control the hydride transfer to  $\text{CO}_2$ .  
27  
28  
29  
30

31 The electrochemical assessment of  $\text{Ru}(\text{CO})(\text{H})^+$  indicated that its singly-reduced form was stable  
32 under the electrochemical timescales of cyclic voltammetry and controlled potential electrolysis  
33 experiments. The photochemically generated  $\text{Ru}(\text{CO})(\text{H})^0$  further supported this observation by showing  
34 the long-lasting formation of  $\text{Ru}(\text{CO})(\text{H})^0$  under inert  $\text{N}_2$  conditions, with no indication of side reactivity  
35 with solvent, BIH,  $\text{BIH}^+$  or TBAHCOO salts. Once the stability of  $\text{Ru}(\text{CO})(\text{H})^0$  had been verified,  
36 controlled titrations of  $\text{CO}_2$  to the photochemically generated  $\text{Ru}(\text{CO})(\text{H})^0$  allowed for the quantitative  
37 determination of the rate constant for hydride transfer to  $\text{CO}_2$ ,  $k_{\text{HT}} = 9.6 \text{ M}^{-1} \text{ s}^{-1}$ . This result alone does not  
38 provide sufficient insight into the pathway undertaken for the formation of the O-bound formate product.  
39 Theoretical calculations performed for  $\text{Ru}(\text{CO})(\text{H})^0$  indicated a stepwise pathway for hydride transfer,  
40 Scheme 4. The H-bound formate intermediate is transiently formed after the nucleophilic attack of  $\text{CO}_2$   
41 by the metal hydride, followed by rotational rearrangement to generate the O-bound formate product.  
42  
43  
44  
45  
46  
47  
48  
49  
50  
51  
52  
53  
54  
55  
56  
57  
58  
59  
60

Scheme 4. DFT-computed free energies for hydride transfer to CO<sub>2</sub>.

Comparison of the measured rate constant for Ru(CO)(H)<sup>0</sup> with that obtained for the Ru(tpy)(bpy)(H)<sup>+</sup> metal hydride,  $k_{\text{HT}} = 1.82 \times 10^{-2} \text{ M}^{-1} \text{ s}^{-1}$ ,<sup>56</sup> revealed that even though the free energy change for Ru(CO)(H)<sup>0</sup> to react with CO<sub>2</sub> to generate an O-bound formate is thermodynamically less favorable when compared to Ru(tpy)(bpy)(H)<sup>+</sup>, it does so three-orders of magnitude faster when compared to Ru(tpy)(bpy)(H)<sup>+</sup>, for the same reaction with a similar mechanistic pathway.<sup>57, 60</sup> This difference in kinetic behavior is one example showing that metal hydride reactivity may not simply be determined based on pure thermodynamic predictions, such as those outlined in the diagram in Scheme 3.

The results and discussions have so far demonstrated that TEOA is the major proton source in photochemical assays conducted in CH<sub>3</sub>CN containing BIH or BNAH as the sacrificial electron donor. It was also demonstrated that TEOA is capable of capturing CO<sub>2</sub> in CH<sub>3</sub>CN solution to form the zwitterionic alkylcarbonate adduct, CO<sub>2</sub>-TEOA, with an equilibrium constant of 0.07 M<sup>-1</sup>. This translates into about 20 mM of the CO<sub>2</sub>-TEOA present in solution at saturation concentrations of free CO<sub>2</sub>. The possibility of capturing CO<sub>2</sub> into non-gaseous products is by itself very interesting, but combining the capture of CO<sub>2</sub> with its reduction is strategically advantageous in terms of reducing the energy requirements to perform both steps separately. Only a limited number of studies have reported an acceleration in the reduction of CO<sub>2</sub> via hydrogenation pathways in the presence of bases and alcohols, that presumably contained carbonate, carbamate or alkylcarbonate forms of captured CO<sub>2</sub>.<sup>61-62</sup> Yet, it remains controversial whether the captured form of CO<sub>2</sub> is actively being reduced, as it exists in dynamic equilibrium with free CO<sub>2</sub> in solution. Recently, the synergistic capture of CO<sub>2</sub> and its reduction were more convincingly speculated for a direct insertion of an alkylcarbonate to a Ru(II) metal-hydride catalyst that resulted in the catalytic production of formate.<sup>63</sup> Here, the question of whether CO<sub>2</sub>-TEOA is actively involved in the reduction of CO<sub>2</sub> to formate catalyzed by the Ru(CO)(H)<sup>0</sup> metal hydride, is experimentally addressed.

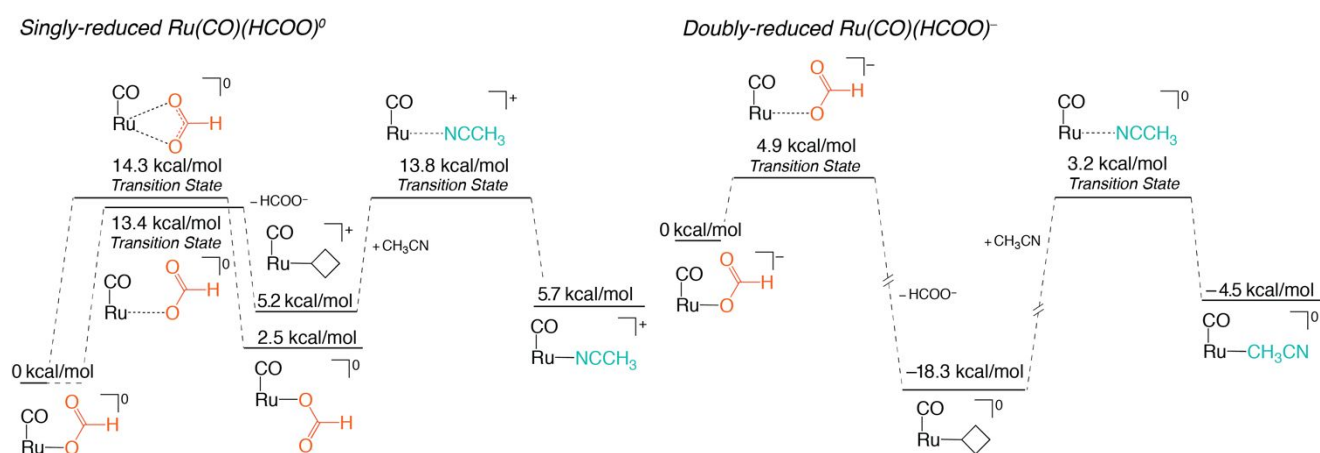
1  
2  
3 When Ru(CO)(H)<sup>0</sup> is photochemically generated in the presence of 1.4 M TEOA, the obtained rate  
4 constant for the formation of the singly-reduced Ru(CO)(HCOO)<sup>0</sup> is unusually enhanced compared to the  
5 hydride transfer step measured in CH<sub>3</sub>CN solutions without TEOA, by about 5 orders of magnitude  
6 relative to the CO<sub>2</sub> concentration, or 6-orders of magnitude if the zwitterionic CO<sub>2</sub>-TEOA concentration  
7 is used. It has been categorically demonstrated that the hydride transfer to CO<sub>2</sub>, for different metal  
8 hydrides, is highly sensitive to the solvation environment, with rate enhancements that span over 2 orders  
9 of magnitude.<sup>53, 56-57</sup> This effect was interpreted as the transition state being stabilized in the reaction  
10 coordinate rather than a change in mechanism in the hydride transfer step. Based on this available  
11 comparison, it would appear somewhat exaggerated to address the 5 orders of magnitude rate enhancement  
12 for Ru(CO)(H)<sup>0</sup> hydride transfer to free CO<sub>2</sub> in 1.4 M TEOA/CH<sub>3</sub>CN simply based on solvent-like effects  
13 in which TEOA stabilizes the transition state. The large disparity in the measured rate constants for  
14 hydride transfer may instead be indicative of a change in mechanism, in which Ru(CO)(H)<sup>0</sup> is being  
15 converted to Ru(CO)(HCOO)<sup>0</sup> in the presence of TEOA. For that, one must consider the pre-activated  
16 C=O bonds of the CO<sub>2</sub>-TEOA zwitterion.  
17  
18  
19  
20  
21  
22  
23  
24  
25  
26  
27

28 Note that bending the CO<sub>2</sub> molecule from its original linear equilibrium geometry pre-activates CO<sub>2</sub>  
29 by making the carbon atom more electrophilic. Under this condition, hydride transfer becomes both  
30 thermodynamically and kinetically more favorable. Unfortunately, activated CO<sub>2</sub> does not spontaneously  
31 exist. Although carbamates and alkylcarbonates, which includes the CO<sub>2</sub>-TEOA zwitterion, are  
32 recognized strategies to activate the C=O bonds, the electron-enriched CO<sub>2</sub>-carbon makes it a poorer  
33 electrophile and consequently makes the hydride transfer thermodynamically more demanding. Therefore,  
34 the formation of Ru(CO)(HCOO)<sup>0</sup> from the hydrido catalyst with the zwitterionic CO<sub>2</sub>-TEOA may not  
35 proceed through a direct hydride transfer pathway. Instead, a concerted CO<sub>2</sub>-TEOA insertion/hydride  
36 transfer pathway may provide a thermodynamically inexpensive and kinetically faster alternative for the  
37 overall conversion of CO<sub>2</sub> to formate. Taken altogether, the results presented herein provide strong  
38 evidence that captured CO<sub>2</sub> in the form of an alkylcarbonate is a promising alternative to access  
39 thermodynamically and kinetically more favorable pathways for the reduction of CO<sub>2</sub> to formate, provided  
40 that the metal hydride catalyst is sufficiently hydridic and not too sterically congested to allow for the  
41 inner sphere interaction between the metal and the captured form of CO<sub>2</sub>.  
42  
43  
44  
45  
46  
47  
48  
49  
50  
51

52 **Formate dissociation.** Electrochemical studies of the *formato* complex in CH<sub>3</sub>CN have shown that its  
53 singly-reduced form is stable on the cyclic voltammetry timescale, while a second reduction is required  
54 to obtain the formate ion product.<sup>11</sup> The electrochemical and TRIR measurements presented here are in  
55  
56  
57

accordance with these early predictions. DFT calculations showed that complete  $\text{HCOO}^-$  dissociation at the first electron reduction of  $\text{Ru}(\text{CO})(\text{HCOO})^+$  is endergonic by  $\Delta G^\circ = 5.2 \text{ kcal mol}^{-1}$ . However, an attempt to weaken the Ru–O bond may instead result in formation of a bidentate metal-formate with the electron delocalized through the O---Ru---O bonds, which is a transition state in the equilibrium between two O-bound  $\text{Ru}(\text{CO})(\text{HCOO})^0$  isomers, Scheme 5 (left). Photochemically generated  $\text{Ru}(\text{CO})(\text{HCOO})^0$  showed no clear evidence for the dissociation of the bound formate within hundreds of microseconds; an observation that agrees with the sluggish kinetics for the loss of formate obtained from the scan-rate dependent electrochemical data.

Scheme 5. DFT-computed free energies for formate dissociation.



Previous studies on polypyridyl-metal complexes have indicated that placing more electron density at the metal strongly influences the stability of anion ligands.<sup>64</sup> This context supports the electrochemical observations of rapid  $\text{HCOO}^-$  dissociation from the doubly-reduced  $\text{Ru}(\text{CO})(\text{HCOO})^-$ . Once  $\text{HCOO}^-$  dissociates, the six coordinate  $\text{Ru}(\text{CO})(\text{CH}_3\text{CN})^0$  may exist transiently and in thermal equilibrium with the five-coordinate  $\text{Ru}(\text{CO})^0$  complex in the absence of proton sources, Scheme 5 (right). In fact, the computed endergonic free energy change,  $\Delta G^\circ = 13.8 \text{ kcal mol}^{-1}$ , for this reaction equilibrium  $\text{Ru}(\text{CO})^0 + \text{CH}_3\text{CN} \rightleftharpoons \text{Ru}(\text{CO})(\text{CH}_3\text{CN})^0$  implicates the five-coordinate  $\text{Ru}(\text{CO})^0$  as the most probable transient intermediate in the absence of proton sources. The experimental data gathered from electrochemical and sodium amalgam reductions further support this computational analysis.

As described in the Results section, electrochemical reduction of  $\text{Ru}(\text{CO})(\text{HCOO})^+$  is irreversible at the first reduction in the presence of TEOA, followed by formation of the metal hydride complex and its subsequent one-electron reduction to  $\text{Ru}(\text{CO})(\text{H})^0$ . Comparative analysis of the extracted rates for the loss

1  
2  
3 of formate indicates that this process occurs 2-orders of magnitude faster in the presence of 50 mM TEOA.  
4 The photochemically generated singly-reduced  $\text{Ru}(\text{CO})(\text{HCOO})^0$  showed time-dependent absorption  
5 changes that were consistent with the formation of the singly-reduced *solvento* complex,  
6  $\text{Ru}(\text{CO})(\text{CH}_3\text{CN})^+$ . This result demonstrates that in 1.4 M TEOA/ $\text{CH}_3\text{CN}$  solution, the partial loss of  
7 formate and subsequent coordination of a solvent molecule to the metal occurred in a few microseconds  
8 ( $\tau = 1.8 \mu\text{s}$ ). The facilitated dissociation of  $\text{HCOO}^-$  at the first reduction of  $\text{Ru}(\text{CO})(\text{HCOO})^+$  in the  
9 presence of TEOA is understood here by means of hydrogen bonding interactions that stabilize the  
10 dissociation step and the anionic products.  
11  
12  
13  
14  
15  
16

## 17 18 CONCLUSION

19  
20 Electrochemical and spectroscopic investigations of Ru(II) carbonyl complexes have guided the study  
21 of the transient intermediates in the photochemical reduction of  $\text{CO}_2$  to formate in  $\text{CH}_3\text{CN}$  solution. The  
22 persistent nature of one carbonyl ligand allowed for the characterization of different variations of the  
23 Ru(II) carbonyl complexes based on their expected roles in the catalytic cycle for formate production.  
24 Electrochemistry and sodium-amalgam reductions provided direct evidence of the unsaturated, five-  
25 coordinate nature of the  $[\text{Ru}(\text{dmb})(\text{CO})]^0$  complex – a highly reactive intermediate believed to precede  
26 the  $\text{CO}_2$  binding step or the protonation of the metal. Spectroelectrochemical methods showed that the  
27 *hydrido* complex is formed after reduction of the *solvento* and *formato* complexes even without an added  
28 proton source, and this effect is enhanced when TEOA is present. TRIR measurements in the carbonyl  
29 stretching infrared region were used to time-resolve transient intermediates known in the catalytic cycle  
30 for  $\text{CO}_2$  reduction to formate. The sluggish kinetics of the deprotonation of  $\text{BIH}^{*+}$  by TEOA in  $\text{CH}_3\text{CN}$   
31 represents the major loss of solar energy conversion as only about 10% of the total reduced catalytic  
32 species survive to time scales necessary for chemical transformations. On a positive note, TEOA has the  
33 surprising ability to capture  $\text{CO}_2$  in the form of a Zwitterionic adduct, and contrary to a previously held  
34 assumption that its main role is to act as a simple Brønsted base to deprotonate  $\text{BIH}^{*+}$ , it actively  
35 participates in and enhances key catalytic steps: i) TEOA is the proton source for metal hydride  
36 regeneration, ii) TEOA significantly enhances, by 6-orders of magnitude, the rate constant for hydride  
37 transfer to  $\text{CO}_2$  through the Zwitterionic-captured  $\text{CO}_2$ , and iii) TEOA promotes fast dissociation of  
38 formate product from the singly-reduced form of the O-bound *formato* complex, while two electrons are  
39 generally required for the same reaction in the absence of TEOA. Although this study focuses on a specific  
40  
41  
42  
43  
44  
45  
46  
47  
48  
49  
50  
51  
52  
53  
54  
55  
56  
57  
58  
59  
60

class of catalysts, the results presented herein are broadly applicable and their implications to CO<sub>2</sub> reduction to formate should be considered when proposing reaction pathways and mechanisms.

## ASSOCIATED CONTENT

### Supporting Information

Additional spectroscopic and electrochemical characterizations; thermochemical cycles used for hydricity and pK<sub>a</sub> calculations; and Cartesian coordinates of the optimized DFT structures. This material is available free of charge via the Internet at <http://pubs.acs.org/>.

## AUTHOR INFORMATION

### Corresponding authors

\*E-mail: [fujita@bnl.gov](mailto:fujita@bnl.gov), [renatons@bnl.gov](mailto:renatons@bnl.gov)

### ORCID

Renato N. Sampaio: 0000-0002-7158-6470

David C. Grills: 0000-0001-8349-9158

Dmitry E. Polyansky: 0000-0002-0824-2296

David J. Szalda: 0000-0002-6219-2429

Etsuko Fujita: 0000-0002-0407-6307

## ACKNOWLEDGEMENTS

This work was supported by the U.S. Department of Energy, Office of Science, Office of Basic Energy Sciences, Division of Chemical Sciences, Geosciences, & Bioscience, under contract DE-SC0012704. We thank Dr. Javier Concepcion (BNL), Dr. Gerald Manbeck (BNL), Dr. Mehmed Z. Ertem (BNL), and Prof. Osamu Ishitani (Tokyo Institute of Technology) for helpful discussions, especially Dr. Ertem for his assistance with DFT calculation analysis.

## REFERENCES

- (1) Yamazaki, Y.; Takeda, H.; Ishitani, O., Photocatalytic Reduction of CO<sub>2</sub> Using Metal Complexes. *J. Photochem. Photobiol. C* **2015**, *25*, 106-137.
- (2) Kuramochi, Y.; Ishitani, O.; Ishida, H., Reaction Mechanisms of Catalytic Photochemical CO<sub>2</sub> Reduction Using Re(I) and Ru(II) Complexes. *Coord. Chem. Rev.* **2018**, *373*, 333-356.
- (3) Pellegrin, Y.; Odobel, F., Sacrificial Electron Donor Reagents for Solar Fuel Production. *Comptes Rendus Chimie* **2017**, *20*, 283-295.
- (4) Tamaki, Y.; Ishitani, O., Supramolecular Photocatalysts for the Reduction of CO<sub>2</sub>. *ACS Catal.* **2017**, *7*, 3394-3409.

- (5) Morimoto, T.; Nakajima, T.; Sawa, S.; Nakanishi, R.; Imori, D.; Ishitani, O., CO<sub>2</sub> Capture by a Rhenium(I) Complex with the Aid of Triethanolamine. *J. Am. Chem. Soc.* **2013**, *135*, 16825-16828.
- (6) Koizumi, H.; Chiba, H.; Sugihara, A.; Iwamura, M.; Nozaki, K.; Ishitani, O., CO<sub>2</sub> Capture by Mn(I) and Re(I) Complexes with a Deprotonated Triethanolamine Ligand. *Chem. Sci.* **2019**, *10*, 3080-3088.
- (7) Queyriaux, N.; Swords, W. B.; Agarwala, H.; Johnson, B. A.; Ott, S.; Hammarström, L., Mechanistic Insights on the Non-Innocent Role of Electron Donors: Reversible Photocapture of CO<sub>2</sub> by Ru<sup>II</sup>-Polypyridyl Complexes. *Dalton Trans.* **2019**, *48*, 16894-16898.
- (8) Ishida, H.; Tanaka, K.; Tanaka, T., Electrochemical CO<sub>2</sub> Reduction Catalyzed by Ruthenium Complexes [Ru(bpy)<sub>2</sub>(CO)<sub>2</sub>]<sup>2+</sup> and [Ru(bpy)<sub>2</sub>(CO)Cl]<sup>+</sup>. Effect of pH on the Formation of CO and HCOO. *Organometallics* **1987**, *6*, 181-186.
- (9) Ishida, H.; Terada, T.; Tanaka, K.; Tanaka, T., Photochemical Carbon Dioxide Reduction Catalyzed by [Ru(bpy)<sub>2</sub>(CO)<sub>2</sub>]<sup>2+</sup> Using Triethanolamine and 1-benzyl-1,4-Dihydronicotinamide as an Electron Donor. *Inorg. Chem.* **1990**, *29*, 905-911.
- (10) Lehn, J.-M.; Ziessel, R., Photochemical Reduction of Carbon Dioxide to Formate Catalyzed by 2,2'-bipyridine- or 1,10-phenanthroline-Ruthenium(II) Complexes. *J. Organomet. Chem.* **1990**, *382*, 157-173.
- (11) Pugh, J. R.; Bruce, M. R. M.; Sullivan, B. P.; Meyer, T. J., Formation of a Metal-Hydride Bond and the Insertion of Carbon Dioxide. Key Steps in the Electrocatalytic Reduction of Carbon Dioxide to Formate Anion. *Inorg. Chem.* **1991**, *30*, 86-91.
- (12) Nakajima, H.; Tsuge, K.; Toyohara, K.; Tanaka, K., Stabilization of [Ru(bpy)<sub>2</sub>(CO)(η<sup>1</sup>-CO<sub>2</sub>)] and Unprecedented Reversible Oxide Transfer Reactions from CO<sub>3</sub><sup>2-</sup> to [Ru(bpy)<sub>2</sub>(CO)<sub>2</sub>]<sup>2+</sup> and from [Ru(bpy)<sub>2</sub>(CO)(η<sup>1</sup>-CO<sub>2</sub>)] to CO<sub>2</sub>. *J. Organomet. Chem.* **1998**, *569*, 61-69.
- (13) Fujita, E.; Chou, M.; Tanaka, K., Characterization of Ru(bpy)<sub>2</sub>(CO)(COO) Prepared by CO<sub>2</sub> Addition to Ru(bpy)<sub>2</sub>(CO) in Acetonitrile. *App. Organomet. Chem.* **2000**, *14*, 844-846.
- (14) Tamaki, Y.; Morimoto, T.; Koike, K.; Ishitani, O., Photocatalytic CO<sub>2</sub> Reduction with High Turnover Frequency and Selectivity of Formic Acid Formation Using Ru(II) Multinuclear Complexes. *Proc. Natl. Acad. Sci. USA* **2012**, *109*, 15673-15678.
- (15) Kobayashi, K.; Tanaka, K., Approach to Multi-Electron Reduction Beyond Two-Electron Reduction of CO<sub>2</sub>. *Phys. Chem. Chem. Phys.* **2014**, *16*, 2240-2250.
- (16) Cheng, S. C.; Blaine, C. A.; Hill, M. G.; Mann, K. R., Electrochemical and IR Spectroelectrochemical Studies of the Electrocatalytic Reduction of Carbon Dioxide by [Ir<sub>2</sub>(dimen)<sub>4</sub>]<sup>2+</sup> (dimen = 1,8-Diisocyanomenthane). *Inorg. Chem.* **1996**, *35*, 7704-7708.
- (17) Sullivan, B. P.; Caspar, J. V.; Meyer, T. J.; Johnson, S., Hydrido Carbonyl Complexes of Osmium(II) and Ruthenium(II) Containing Polypyridyl Ligands. *Organometallics* **1984**, *3*, 1241-1251.
- (18) Ishida, H.; Tanaka, K.; Morimoto, M.; Tanaka, T., Isolation of Intermediates in the Water Gas Shift Reactions Catalyzed by [Ru(bpy)<sub>2</sub>(CO)Cl]<sup>+</sup> and [Ru(bpy)<sub>2</sub>(CO)<sub>2</sub>]<sup>2+</sup>. *Organometallics* **1986**, *5*, 724-730.
- (19) Kelly, J. M.; Vos, J. G., cis-[Ru(bpy)<sub>2</sub>(CO)H]<sup>+</sup>— A Possible Intermediate in the Photochemical Production of H<sub>2</sub> from Water Catalyzed by [Ru(bpy)<sub>3</sub>]<sup>2+</sup>? *Angew. Chem. Int. Ed.* **1982**, *21*, 628-629.
- (20) Kelly, J. M.; O'Connell, C. M.; Vos, J. G., Preparation, Spectroscopic Characterisation, Electrochemical and Photochemical Properties of cis-bis(2,2'-bipyridyl)carbonylruthenium(II) Complexes. *J. Chem. Soc., Dalton Trans.* **1986**, 253-258.
- (21) Fuentes, M. J.; Bognanno, R. J.; Dougherty, W. G.; Boyko, W. J.; Scott Kassel, W.; Dudley, T. J.; Paul, J. J., Structural, Electronic and Acid/Base Properties of [Ru(bpy(OH)<sub>2</sub>)<sub>3</sub>]<sup>2+</sup> (bpy(OH)<sub>2</sub> = 4,4'-dihydroxy-2,2'-bipyridine). *Dalton Trans.* **2012**, *41*, 12514-12523.
- (22) Pavlishchuk, V.; Addison, A. W., Conversion Constants for Redox Potentials Measured Versus Different Reference Electrodes in Acetonitrile Solutions at 25°C. *Inorg. Chim. Acta.* **2000**, *298*, 97-102.

- (23) BASi DigiSim® Simulation Software for Cyclic Voltammetry. <http://www.basinc.com/products/ec/digisim/>.
- (24) Grills, D. C.; Farrington, J. A.; Layne, B. H.; Preses, J. M.; Bernstein, H. J.; Wishart, J. F., Development of Nanosecond Time-Resolved Infrared Detection at the LEAF Pulse Radiolysis Facility. *Rev. Sci. Instrum.* **2015**, *86*, 044102.
- (25) Frisch, M. J.; Trucks, G. W.; Schlegel, H. B.; Scuseria, G. E.; Robb, M. A.; Cheeseman, J. R.; Scalmani, G.; Barone, V.; Petersson, G. A.; Nakatsuji, H.; Li, X.; Caricato, M.; Marenich, A. V.; Bloino, J.; Janesko, B. G.; Gomperts, R.; Mennucci, B.; Hratchian, H. P.; Ortiz, J. V.; Izmaylov, A. F.; Sonnenberg, J. L.; Williams, D.; Ding, F.; Lipparini, F.; Egidi, F.; Goings, J.; Peng, B.; Petrone, A.; Henderson, T.; Ranasinghe, D.; Zakrzewski, V. G.; Gao, J.; Rega, N.; Zheng, G.; Liang, W.; Hada, M.; Ehara, M.; Toyota, K.; Fukuda, R.; Hasegawa, J.; Ishida, M.; Nakajima, T.; Honda, Y.; Kitao, O.; Nakai, H.; Vreven, T.; Throssell, K.; Montgomery Jr., J. A.; Peralta, J. E.; Ogliaro, F.; Bearpark, M. J.; Heyd, J. J.; Brothers, E. N.; Kudin, K. N.; Staroverov, V. N.; Keith, T. A.; Kobayashi, R.; Normand, J.; Raghavachari, K.; Rendell, A. P.; Burant, J. C.; Iyengar, S. S.; Tomasi, J.; Cossi, M.; Millam, J. M.; Klene, M.; Adamo, C.; Cammi, R.; Ochterski, J. W.; Martin, R. L.; Morokuma, K.; Farkas, O.; Foresman, J. B.; Fox, D. J. *Gaussian 16 Rev. C.01*, Wallingford, CT, 2016.
- (26) Zhao, Y.; Truhlar, D. G., The M06 Suite of Density Functionals for Main Group Thermochemistry, Thermochemical Kinetics, Noncovalent Interactions, Excited States, and Transition Elements: Two New Functionals and Systematic Testing of Four M06-Class Functionals and 12 Other Functionals. *Theor. Chem. Acc.* **2008**, *120*, 215-241.
- (27) Tomasi, J.; Mennucci, B.; Cammi, R., Quantum Mechanical Continuum Solvation Models. *Chem. Rev.* **2005**, *105*, 2999-3094.
- (28) Hay, P. J.; Wadt, W. R., Ab Initio Effective Core Potentials for Molecular Calculations. Potentials for K to Au Including the Outermost Core Orbitals. *J. Chem. Phys.* **1985**, *82*, 299-310.
- (29) Roy, L. E.; Hay, P. J.; Martin, R. L., Revised Basis Sets for the LANL Effective Core Potentials. *J. Chem. Theory Comput.* **2008**, *4*, 1029-1031.
- (30) Tamaki, Y.; Koike, K.; Ishitani, O., Highly Efficient, Selective, and Durable Photocatalytic System for CO<sub>2</sub> Reduction to Formic Acid. *Chem. Sci.* **2015**, *6*, 7213-7221.
- (31) Heldebrant, D. J.; Koech, P. K.; Ang, M. T. C.; Liang, C.; Rainbolt, J. E.; Yonker, C. R.; Jessop, P. G., Reversible Zwitterionic Liquids, the Reaction of Alkanol Guanidines, Alkanol Amidines, and Diamines with CO<sub>2</sub>. *Green Chem.* **2010**, *12*, 713-721.
- (32) Phan, L.; Chiu, D.; Heldebrant, D. J.; Huttenhower, H.; John, E.; Li, X.; Pollet, P.; Wang, R.; Eckert, C. A.; Liotta, C. L.; Jessop, P. G., Switchable Solvents Consisting of Amidine/Alcohol or Guanidine/Alcohol Mixtures. *Ind. Eng. Chem. Res.* **2008**, *47*, 539-545.
- (33) Kortunov, P. V.; Siskin, M.; Paccagnini, M.; Thomann, H., CO<sub>2</sub> Reaction Mechanisms with Hindered Alkanolamines: Control and Promotion of Reaction Pathways. *Energy & Fuels* **2016**, *30*, 1223-1236.
- (34) Heldebrant, D. J.; Yonker, C. R.; Jessop, P. G.; Phan, L., Organic Liquid CO<sub>2</sub> Capture Agents with High Gravimetric CO<sub>2</sub> Capacity. *Energy Environ. Sci.* **2008**, *1*, 487-493.
- (35) Kortunov, P. V.; Siskin, M.; Baugh, L. S.; Calabro, D. C., In Situ Nuclear Magnetic Resonance Mechanistic Studies of Carbon Dioxide Reactions with Liquid Amines in Aqueous Systems: New Insights on Carbon Capture Reaction Pathways. *Energy & Fuels* **2015**, *29*, 5919-5939.
- (36) Tamaki, Y.; Koike, K.; Morimoto, T.; Ishitani, O., Substantial Improvement in the Efficiency and Durability of a Photocatalyst for Carbon Dioxide Reduction Using a Benzoimidazole Derivative as an Electron Donor. *J. Catal.* **2013**, *304*, 22-28.

- (37) Zhu, X.-Q.; Zhang, M.-T.; Yu, A.; Wang, C.-H.; Cheng, J.-P., Hydride, Hydrogen Atom, Proton, and Electron Transfer Driving Forces of Various Five-Membered Heterocyclic Organic Hydrides and Their Reaction Intermediates in Acetonitrile. *J. Am. Chem. Soc.* **2008**, *130*, 2501-2516.
- (38) Ilic, S.; Pandey Kadel, U.; Basdogan, Y.; Keith, J. A.; Glusac, K. D., Thermodynamic Hydricities of Biomimetic Organic Hydride Donors. *J. Am. Chem. Soc.* **2018**, *140*, 4569-4579.
- (39) Izutsu, K.; Nakamura, T.; Takizawa, K.; Takeda, A., Calorimetric Determination of Thermodynamic Parameters for the Dissociations of Acids in Dipolar Aprotic Solvents. *Bull. Chem. Soc., Jpn.* **1985**, *58*, 455-458.
- (40) Kaljurand, I.; Kütt, A.; Sooväli, L.; Rodima, T.; Mäemets, V.; Leito, I.; Koppel, I. A., Extension of the Self-Consistent Spectrophotometric Basicity Scale in Acetonitrile to a Full Span of 28 pKa Units: Unification of Different Basicity Scales. *J. Org. Chem.* **2005**, *70*, 1019-1028.
- (41) Matsubara, Y.; Grills, D. C.; Koide, Y., Thermodynamic Cycles Relevant to Hydrogenation of CO<sub>2</sub> to Formic Acid in Water and Acetonitrile. *Chem. Lett.* **2019**, *48*, 627-629.
- (42) Pschenitza, M.; Meister, S.; Rieger, B., Positive Effect of 1,8-diazabicyclo[5.4.0]undec-7-ene (DBU) on Homogeneous Photocatalytic Reduction of CO<sub>2</sub>. *Chem. Commun.* **2018**, *54*, 3323-3326.
- (43) Chardon-Noblat, S.; Collomb-Dunand-Sauthier, M. N.; Deronzier, A.; Ziessel, R.; Zsoldos, D., Formation of Polymeric [ $\text{Ru}^0(\text{bpy})(\text{CO})_2$ ]<sub>n</sub> Films by Electrochemical Reduction of  $[\text{Ru}(\text{bpy})_2(\text{CO})_2](\text{PF}_6)_2$ : Its Implication in CO<sub>2</sub> Electrocatalytic Reduction. *Inorg. Chem.* **1994**, *33*, 4410-4412.
- (44) Machan, C. W.; Sampson, M. D.; Kubiak, C. P., A Molecular Ruthenium Electrocatalyst for the Reduction of Carbon Dioxide to CO and Formate. *J. Am. Chem. Soc.* **2015**, *137*, 8564-8571.
- (45) Ceballos, B. M.; Yang, J. Y., Directing the Reactivity of Metal Hydrides for Selective CO<sub>2</sub> Reduction. *Proc. Natl. Acad. Sci. USA* **2018**, *115*, 12686-12691.
- (46) Wiedner, E. S.; Chambers, M. B.; Pitman, C. L.; Bullock, R. M.; Miller, A. J. M.; Appel, A. M., Thermodynamic Hydricity of Transition Metal Hydrides. *Chem. Rev.* **2016**, *116*, 8655-8692.
- (47) Hu, Y.; Norton, J. R., Kinetics and Thermodynamics of H<sup>-</sup>/H<sup>•</sup>/H<sup>+</sup> Transfer from a Rhodium(III) Hydride. *J. Am. Chem. Soc.* **2014**, *136*, 5938-5948.
- (48) Garg, K.; Matsubara, Y.; Ertem, M. Z.; Lewandowska-Andralojc, A.; Sato, S.; Szalda, D. J.; Muckerman, J. T.; Fujita, E., Striking Differences in Properties of Geometric Isomers of  $[\text{Ir}(\text{tpy})(\text{ppy})\text{H}]^+$ : Experimental and Computational Studies of their Hydricities, Interaction with CO<sub>2</sub>, and Photochemistry. *Angew. Chem. Int. Ed.* **2015**, *54*, 14128-14132.
- (49) Waldie, K. M.; Ostericher, A. L.; Reineke, M. H.; Sasayama, A. F.; Kubiak, C. P., Hydricity of Transition-Metal Hydrides: Thermodynamic Considerations for CO<sub>2</sub> Reduction. *ACS Catal.* **2018**, *8*, 1313-1324.
- (50) Felton, G. A. N.; Vannucci, A. K.; Okumura, N.; Lockett, L. T.; Evans, D. H.; Glass, R. S.; Lichtenberger, D. L., Hydrogen Generation from Weak Acids: Electrochemical and Computational Studies in the  $[(\eta^5\text{-C}_5\text{H}_5)\text{Fe}(\text{CO})_2]_2$  System. *Organometallics* **2008**, *27*, 4671-4679.
- (51) Sullivan, B. P.; Bolinger, C. M.; Conrad, D.; Vining, W. J.; Meyer, T. J., One- and Two-Electron Pathways in the Electrocatalytic Reduction of CO<sub>2</sub> by fac-Re(bpy)(CO)<sub>3</sub>Cl (bpy = 2,2'-bipyridine). *J. Chem. Soc., Chem. Commun.* **1985**, 1414-1416.
- (52) Hazari, N.; Heimann, J. E., Carbon Dioxide Insertion into Group 9 and 10 Metal-Element  $\sigma$  Bonds. *Inorg. Chem.* **2017**, *56*, 13655-13678.
- (53) Heimann, J. E.; Bernskoetter, W. H.; Hazari, N.; Mayer, J. M., Acceleration of CO<sub>2</sub> Insertion Into Metal Hydrides: Ligand, Lewis Acid, and Solvent Effects on Reaction Kinetics. *Chem. Sci.* **2018**, *9*, 6629-6638.

- 1  
2  
3 (54) Kern, S.; van Eldik, R., Mechanistic Insight from Activation Parameters for the Reaction of a  
4 Ruthenium Hydride Complex with CO<sub>2</sub> in Conventional Solvents and an Ionic Liquid. *Inorg. Chem.* **2012**,  
5 *51*, 7340-7345.  
6  
7 (55) Creutz, C.; Chou, M. H., Rapid Transfer of Hydride Ion from a Ruthenium Complex to C<sub>1</sub> Species  
8 in Water. *J. Am. Chem. Soc.* **2007**, *129*, 10108-10109.  
9 (56) Konno, H.; Kobayashi, A.; Sakamoto, K.; Fagalde, F.; Katz, N. E.; Saitoh, H.; Ishitani, O., Synthesis  
10 and Properties of [Ru(tpy)(4,4'-X<sub>2</sub>bpy)H]<sup>+</sup> (tpy = 2,2':6',2''-terpyridine, bpy = 2,2'-bipyridine, X = H and  
11 MeO), and their Reactions with CO<sub>2</sub>. *Inorg. Chim. Acta.* **2000**, *299*, 155-163.  
12 (57) Heimann, J. E.; Bernskoetter, W. H.; Hazari, N., Understanding the Individual and Combined Effects  
13 of Solvent and Lewis Acid on CO<sub>2</sub> Insertion into a Metal Hydride. *J. Am. Chem. Soc.* **2019**, *141*, 10520-  
14 10529.  
15 (58) Huang, J.; Chen, J.; Gao, H.; Chen, L., Kinetic Aspects for the Reduction of CO<sub>2</sub> and CS<sub>2</sub> with  
16 Mixed-Ligand Ruthenium(II) Hydride Complexes Containing Phosphine and Bipyridine. *Inorg. Chem.*  
17 **2014**, *53*, 9570-9580.  
18 (59) Sullivan, B. P.; Meyer, T. J., Kinetics and Mechanism of Carbon Dioxide Insertion into a Metal-  
19 Hydride Bond. A Large Solvent Effect and an Inverse Kinetic Isotope Effect. *Organometallics* **1986**, *5*,  
20 1500-1502.  
21 (60) Creutz, C.; Chou, M. H.; Hou, H.; Muckerman, J. T., Hydride Ion Transfer from Ruthenium(II)  
22 Complexes in Water: Kinetics and Mechanism. *Inorg. Chem.* **2010**, *49*, 9809-9822.  
23 (61) Jessop, P. G.; Ikariya, T.; Noyori, R., Homogeneous Hydrogenation of Carbon Dioxide. *Chem. Rev.*  
24 **1995**, *95*, 259-272.  
25 (62) Munshi, P.; Main, A. D.; Linehan, J. C.; Tai, C.-C.; Jessop, P. G., Hydrogenation of Carbon Dioxide  
26 Catalyzed by Ruthenium Trimethylphosphine Complexes: The Accelerating Effect of Certain Alcohols  
27 and Amines. *J. Am. Chem. Soc.* **2002**, *124*, 7963-7971.  
28 (63) Lao, D. B.; Galan, B. R.; Linehan, J. C.; Heldebrant, D. J., The Steps of Activating a Prospective  
29 CO<sub>2</sub> Hydrogenation Catalyst with Combined CO<sub>2</sub> Capture and Reduction. *Green Chem.* **2016**, *18*, 4871-  
30 4874.  
31 (64) Sullivan, B. P.; Conrad, D.; Meyer, T. J., Chemistry of Highly Reduced Polypyridyl-Metal  
32 Complexes. Anion Substitution Induced by Ligand-Based Reduction. *Inorg. Chem.* **1985**, *24*, 3640-3645.  
33  
34  
35  
36  
37  
38  
39  
40  
41  
42  
43  
44  
45  
46  
47  
48  
49  
50  
51  
52  
53  
54  
55  
56  
57  
58  
59  
60

## TOC

